Enhancing Resilience of Urban Electric-Road-Metro Interdependent Network Considering Electric Bus Scheduling

Gengming Liu, Rui Cheng, *Member*, *IEEE*, Wenxia Liu, *Member*, *IEEE* Qingxin Shi, *Member*, *IEEE* Zhaoyu Wang, *Senior Member*, *IEEE*

***Abstract*—With the increasing electrification of urban transportation, urban power and traffic systems are highly coupled and influence each other, leading to a challenge for the post-event resilience enhancement of urban electric-traffic interdependent network (ETIN). In this context, we propose a multi-layer electric-metro-road interdependent network where the metro network (MN) depends on the distribution power network (DPN) and interacts with the road traffic network (RTN) synchronously. Electric buses (EBs), as one public dispatchable resource, are considered and explored to provide bridging routes for disabled MNs and supply power for failed DPNs, with consideration of three different service trips, i.e., the original trip, bridging trip, and charge-discharge trip. On this basis, a spatio-temporal network-based EB route schedule model is constructed. To consider the evacuation demand of affected MN routes, a fast DPN restoration strategy is proposed to minimize the time cost of lost load by integrating the network reconfiguration with the collaborative allocation of repair crews (RCs) and EBs. Finally, a distributed method is further devised for the coordination among different stakeholders. The proposed method is verified on two electric-traffic systems to show that the collaborative scheduling of RCs and EBs can effectively enhance the resilience of ETIN under metro service disruptions.**

***Index Terms*—Electric-traffic interdependent network, electric bus scheduling, load restoration, multi-layer interdependent network, resilience.**

NOMENCLATURE

A. Sets

$\mathbf{V_P}, \mathbf{E_P}$	Sets of DPN nodes and DPN lines, indexed by v_p and e_p, respectively;
$\mathbf{V_T}, \mathbf{E_T}$	Sets of TPN nodes and TPN lines, indexed by v_τ and e_τ, respectively;
$\mathbf{V_M}, \mathbf{E_M}$	Sets of MN nodes and MN links, indexed by v_m and e_m, respectively;
$\mathbf{V_R}, \mathbf{E_R}$	Sets of RTN nodes and RTN links, indexed by v_r and e_r, respectively;
$\mathbf{B}$	Set of EBs, indexed by m;
$\mathbf{B_s}$	Set of EBs located in the depot;
$\mathbf{B_w}$	Set of EBs running on the original routes;
$\mathbf{T}$	Set of service trips or nodes of EB's spatial temporal network, indexed by n;
$\mathbf{T_o}$	Set of original trips;
$\mathbf{T_b}$	Set of bridging trips;
$\mathbf{T_c}$	Set of charge-discharge trips;
$\mathbf{A}$	Set of arcs of EB's spatial-temporal network, indexed by *arc*;
$\mathbf{W}$	Set of weights of $\mathbf{A}$, indexed by t_w;
$\mathbf{R_o}$	Set of original routes, indexed by i_o;
$\mathbf{R_b}$	Set of bridging routes, indexed by i_b;
$\mathbf{V_P^C}$	Set of charging stations, indexed by i_c;
$\mathbf{T_{time}}$	Set of time periods, indexed by t;
$\mathbf{V_P^{couple}}$	Set of DPN nodes coupled with MN demand;
$\mathbf{V_P^M}$	Set of DPN nodes connected to the main grid;
$\mathbf{V_P^D}$	Set of DPN nodes connected to DGs;
$\mathbf{V_P^S}$	Set of outputting source DPN nodes;
$\mathbf{S_P}$	Set of fault locations, indexed by s_j;
$\mathbf{C_{re}}$	Set of RCs, indexed by c_i;
$\mathbf{R_m^{out}}$	Set of failed MN routes, indexed by r;

B. Parameters

V_k	Utility value of route k;
DT_k, TT_k	Travel distance and time of route k;
P_k, D_k^t	Chosen probability and assigned demand of route k;
$T_{(s_i,s_j)}^{travel}$	Travel time from s_i to s_j through $Path_{(s_i,s_j)}$;
$t_{n^1}^e$, $t_{n^2}^b$	End time and start time of trip n;
$t_{n^2}^{n^1}$	Transfer time between trip n^1 and n^2;
$\underline{p_m^{\mathrm{ch}}}$, $\overline{p_m^{\mathrm{dch}}}$	Maximum charging/discharging power of EB m;
η_m^{ch}, η_m^{dch}	Charging/discharging efficiency of EB m;
$\mathbf{B_m}$	Battery capacity of EB m;
$\mathbf{N_B}$	Maximum available number of EB;
ϖ_1, ϖ_2	Load importance of node$\mathbf{V_P}/\mathbf{V_P^{couple}}$and $\mathbf{V_P^{couple}}$
δ_1, δ_2	Penalty coefficients in the objective function;

C. Variables

α_m^n	Binary; 1 if EB m is assigned for trip n;
$\alpha_m^{n^1 n^2}$	Binary; 1 if EB m is assigned through arc $\langle n^1, n^2 \rangle$;
β_m^{ch}	Binary; 1 if EB m is charging during trip n
β_m^{dch}	Binary; 1 if EB m is discharging during trip n
p_m^{ch}	Charging power of EB m during trip n;
p_m^{dch}	Discharging power of EB m during trip n;
SOC_m^t	State of charge (SOC) of EB m at t;
$S_{ij,d}^t$	Binary; 1 if the directed line (ij) is closed at t;
$S_{ij,r}^t$	Binary; 1 if the directed line (ji) is closed at t;
f_{ij}^t	Virtual flow from node i to node j at t;

This work was supported in part by the National Natural Science Foundation of China (52307094) and in part by the Fundamental Research Funds for the Central Universities (2023JC008). G. Liu, R. Cheng (corresponding author, ruicheng@ncepu.edu.cn), W. Liu and Q. Shi are with the Dept. of Electrical & Electronics Engineering, North China Electric Power University. Z. Wang is with the Department of Electrical and Computer Engineering, Iowa State University.

z_i^t	Binary; 1 if node i is powered at t;
χ_{c_i,s_j}^t	Binary; 1 if RC c_i is driving to fault s_j or clearing it at t;
$q_{s_j}^t$	Binary; 1 if fault s_j is recovered at t;
$u_{v_{i,p}}$	Binary; 0 if DPN node $v_{i,p}$ fails;
$u_{v_{j,\tau}}$	Binary; 0 if TPN node $v_{j,\tau}$ fails;
$u_{v_{k,m}}$	Binary; 0 if MN node $e_{k,m}$ fails;

I. Introduction

THE rapid development of cities and the growing energy transition accelerate the transportation electrification and Vehicle-to-Grid technology [1]. The Metro network (MN) serves over 50% of traffic volume in megacities ,such as Beijing, China [2]. The number of electric vehicles (EVs) and charging piles in China is estimated to exceed 80 million and 70 million respectively, by 2030 [3], further strengthening the coupling between the urban power network (PN) and traffic network (TN) [4]. On May 18, 2018, the emergency power curtailment of Shenzhen power grid caused nearly 3,000 electric taxis to lose timely charging service and seriously affected the function of road traffic network (RTN) [5]. In 2021, the rainstorm in Zhengzhou, China, caused massive power outages and traffic paralysis, further hindering the urgent repair work of PN [6]. In addition, the prolonged blackouts experienced in Venezuela at 2019 not only led to the interruptions of MNs but also to severe congestion of RTN [7]. In the urban electric-traffic interdependent network (ETIN), the failure of PN could worsen TN that could influence the PN restoration in reverse. In this background, the concept of resilience is introduced to describe the ability of ETIN to survive and quickly recover from unexpected disasters.

The system resilience can be enhanced through pre-event measures before disasters and post-event recovery actions after disasters [8], and the latter is our focus. To enhance PN resilience, recent studies have introduced new approaches alongside traditional methods such as distribution network microgrid (MG) formation [9] and static energy storage deployment [10]. These innovations include the optimal cooperative dispatch of mobile power sources (MPSs) for post-disaster restoration [11]–[13]. Ref. [11] claimed that the EV fleets with flexible charge-discharge behavior can be utilized for MG restoration. A two-stage post-event recovery strategy for the distribution power network (DPN) was proposed in [12], where MPS and repair crew (RC) route planning were modeled based on dynamic traffic assignment. Ref. [13] proposed a collaborative dispatch scheme for various MPSs considering dynamic network reconfiguration. However, the above studies only focused on PN, lacking fault propagation modeling between PN and TN to support the resilience enhancement of urban ETIN.

There have been research works in terms of enhancing the ETIN resilience. Ref [14] studied repair resource allocation under simultaneous faults in DPN and RTN without considering MPS schedule. Ref [15] focused on the post-event DPN restoration through the scheduling of MPSs including private EVs, whereas private EVs cannot be centrally scheduled owing to the owners' private interest. To address this issue, Refs. [16]–[17] considered the participation of public EBs in DPN restoration. However, the interactive fault effects between RTN and DPN were ignored in [14]–[17]. Refs. [18]-[19] modeled the fault propagation between RTN and DPN during the recovery of ETIN. [18] considered the failure of traffic light due to power outage and [19] further considered road blocking owing to a collapsed geographically adjacent power pole. In this scenario, the failed RTN could hinder the timely repair of DPN due to traffic jam or inaccessible repair path. However, they only analyzed the topological connectivity of DPN while simplified the operation model. The operational risk of DPN from EV aggregation charging caused by road disruption [20] or fast charging station (FCS) failure [5], [21] has raised concerns. In such a case, the study in [22] developed a network reconfiguration strategy that coordinates the restoration of DPN and RTN considering EV charging schedule. Current research on ETIN mainly focuses on the coupling between DPN and RTN, using traffic lights as the bridge between them, and the reverse impact of RTN fault on DPN is modeled as delays in the travel of MPS and RC or the EV charging caused by the traffic congestion.

However, none of these works take into account the MN model and its coupled impact in the urban ETIN. The MN is deeply dependent on power supply from DPN [23] and exhibits a complementary relationship with RTN under fault scenarios [24], making it a critical component in the urban TN of ETIN. Most existing post-event measures for enhancing individual MN resilience after interruptions include the optimization of train schedules [25]–[26], transport route scheduling of bridging buses [27] or taxis [28], and resilient energy supply system design against power outage [29]. Nevertheless, an outstanding challenge remains in modeling MN and considering the interactive impact between MN and other networks, including DPN and RTN, in the context of urban ETIN resilience enhancement. There are three major challenges for this problem:

(1) The interdependence of DPN and MN has not been fully explored in the absence of traction power networks (TPN), leaving the failure propagation from DPN to MN unresolved; (2) Redistributing compromised metro passengers during power outage across RTNs and MNs has not been carefully taken into account in the ETIN resilience enhancing problem; (3) The coupling effect among DPN, RTN and MN complicates the collaborative schedule of emergency resources, necessitating an integrated post-event restoration model to enhance the resilience of urban ETIN.

To fill these gaps, we propose a post-disaster resilience enhancement strategy for the urban ETIN, comprising the electric-road-metro interdependent network, with consideration of the extra dual functions of EB under metro disruptions. Our major contributions are summarized as follows:

(1) A multi-layer ETIN model, including *the electric-road-metro interdependent network*, is established. The coupling effect between MN and DPN is modeled through the traction power network (TPN), and the coupling effect between MN and RTN is modeled based on failed load redistribution.

(2) Three types of trips are defined to form the spatial-temporal network of EB, i.e., the original trip for RTN, bridging trip for MN, and charge-discharge trip for RTN. Further-

more, the EB schedule problem (EBSP) is designed to consider the travel transfer among trips and the energy exchange with DPN.

(3) A fast DPN restoration model is proposed to consider the evacuation demand for failed metro lines by integrating the network reconfiguration with the collaborative allocation of RCs and EBs, where auxiliary induce functions (AIFs) are introduced to enhance computational efficiency of mixed integer programming problems. Furthermore, a distributed method is designed for the coordination among various stakeholders.

For the remainder of this paper, the resilience enhancement problem is described in Section II. Section III introduces the models of ETIN and fault propagation within them. Section IV presents the EB route schedule with service trips, and Section V covers DPN restoration with EBs. Section VI reports numerical case studies. Lastly, Section VII concludes this paper.

II. Problem Description

A. Function Analysis for urban EB against Power Outage

With growing concerns about security problems in urban critical infrastructure systems, deliberate attacks on radial urban DPN have posed a significant risk of power outages, impacting the MN and other consumers, which is considered as the extreme event in this paper. Urban EBs, with the dual attributes, i.e., mobile power source and transportation, have enormous potential for enhancing MN and DPN resilience against power outages for the following reasons:

- In cities, the number of EBs is sufficient and far exceeds that of other MPS and can be centrally dispatched by the city bus company compared with private EVs. The widely deployed FCSs can support the charge and discharge of EBs.
- In the urban TN, most EB routes run parallel to the metro lines, and have a higher passenger capacity and lower scheduling costs, compared to other public vehicles (e.g., taxis).

Hence, except for transporting passengers on original routes, two extra functions of EBs are explored, providing bridging routes for suspended MN intervals and supplying power for failed DPNs. These functions are defined as three service trips in this paper.

B. Post-Event Resilience Enhancement of ETIN With EBs

In general, the outage caused by intentionally damaging power lines leads to disrupted metro operations, as depicted in Fig.1. In such situations, restoring power becomes the highest priority in urban emergency management. Alongside dispatching repair crews to the damaged lines, both idle EBs parking at the depot and those already on their original trips, denoted by blue dashed lines, can play the role of MPS to supply power to outage areas. This strategy aids in load recovery for DPN by engaging in charge-discharge trips, indicated by yellow dashed line. Furthermore, these EBs are also used for bridging trips, denoted by wine dashed line, to assist passengers impacted by the disrupted metro intervals.

Hence, the reasonable scheduling of the number and routes of EBs for various service trips, coordination with the RC, and

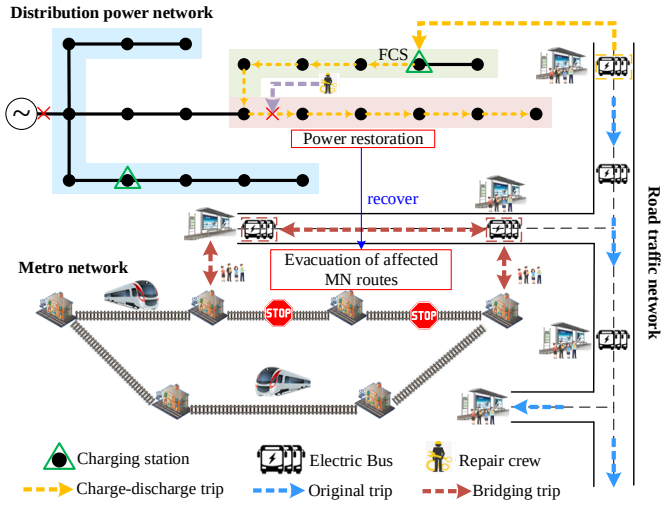

Fig. 1. Problem of enhancing resilience of ETIN considering EBs scheduling

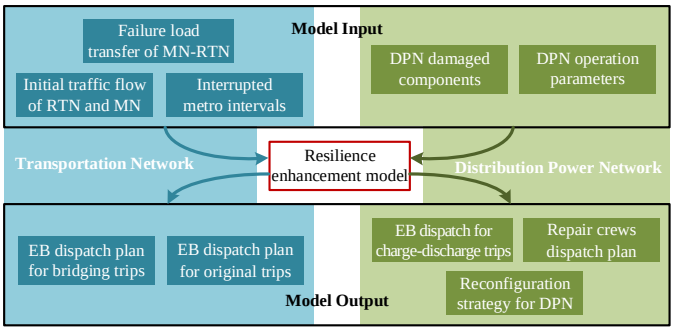

Fig. 2. The framework of optimization model of ETIN resilience enhancement

energy interaction with DPN during emergency restoration are pivotal issues that remain to be addressed in post-disaster resilience enhancement for ETIN. The integrated optimization model framework including inputs and outputs for ETIN resilience enhancement is shown in Fig.2. As the cornerstone of this study, we firstly uncover the failure propagation mechanism of ETIN by modeling the multi-layer electric-metro-road interdependent network, as described in Section III.

III. Modeling Of Multi-Layer Electric-Metro-Road Interdependent Network

The power supply modes for MN are generally divided into centralized one with higher reliability, and distributed one with higher flexibility in the railway expansion. In the centralized metro power supply system, the specialized bulk metro substations supply power for multiple metro substations along a metro line, establishing one-to-X coupling between urban power sources and metro traction stations, while that is one-to-one coupling in the distributed metro power supply system. Additionally, metro lines designed with circular routes can have loop-like TPNs, while those with linear route designs are coupled with chain-like TPNs. Comprising these metro lines and their TPNs, the entire MN and TPN both form a partially meshed network structure.

A. Electric-Metro Interdependent Network

This paper adopts the distributed mode, as depicted in Fig.3. The metro substation connects to the nearest 10 kV source of

urban DPN. The step-down substation transforms 10kV AC power into 400V for station automatic systems, while the traction substation converts it into 1500V DC power for catenaries, from which electric locomotives obtain power. Buses of adjacent metro substations are interconnected to ensure redundancy in power supply for each traction substation and step-down substation. In event of a traction substation failure, the affected catenary can receive power from the traction substation of the adjacent interval through switching operations. Based on this, the tri-layer DPN-TPN-MN interdependent network is proposed in this section.

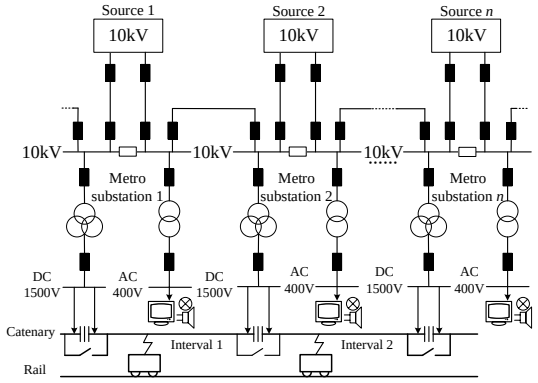

Fig. 3. The schematic diagram of a metro power supply system

1) Topological Interdependence: The 10kV DPN is modeled as a radial network DPN($\mathbf{V_P}, \mathbf{E_P}$). The 10kV TPN is modeled as a partially meshed network TPN($\mathbf{V_T}, \mathbf{E_T}$). The MN is modeled as a partially meshed network MN($\mathbf{V_M}, \mathbf{E_M}$). The graph of tri-layer is shown in Fig.4, where each TPN node $v_{j,t}$ is supplied by a DPN node $v_{i,p}$, i.e., one-to-one coupling, denoted as the interdependent edge $e^{t\leftarrow p}_{j\leftarrow i} = (v_{j,t}, v_{i,p})$. Each MN link $e_{k,m}$ is determined by two TN nodes $v_{j,t} \in \mathbf{V_{j,t}}$, i.e., one-to-two coupling, denoted as the interdependent edge $\mathbf{E}^{t\leftarrow p}_{j\leftarrow i} = (e_{k,m}, \mathbf{V_{j,t}})$.

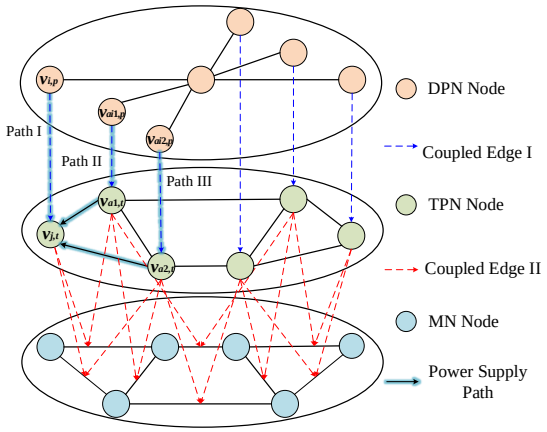

Fig. 4. DPN-TPN-MN tri-layer interdependent network

2) Functional Interdependence: The binary variable $u_{v_{i,p}}$ is used to describe the status of DPN node i.

$$u_{v_{i,p}} = \begin{cases} 0, Deg(v_{i,p}) = 0 \text{ or } P_{i,L} < \xi_p \overline{P_{i,L}} \\ 1, Deg(v_{i,p}) > 0 \text{ and } P_{i,L} \geq \xi_p \overline{P_{i,L}} \end{cases} i \in \mathbf{V_P} \quad (1)$$

where $Deg(v_{i,p})$ denotes the node degree. $P_{i,L}$ and $\overline{P_{i,L}}$ denote the actual load and rated nodal load, respectively. $\xi_p \in [0.5, 1]$ is the tolerance coefficient representing the lowest acceptable load power vacancy ratio. Hence, once the node $v_{i,p}$ is isolated or its load power vacancy ratio is greater than ξ_p, it is assumed to fail.

The status $u_{v_{j,\tau}}$ of TPN node $v_{j,\tau}$ is influenced by the status of the DPN nodes coupled with itself and the supporting capacity of its adjacent TPN nodes.

$$u_{v_{j,\tau}} = \begin{cases} 0, u_{v_{i,p}} = 0 \text{ and } \sum\limits_{a \in \mathbf{A_{j,\tau}}} u_{v_{ai,p}} \leq 1 (v_{j,\tau}, v_{i,p}) = e^{j\leftarrow i}_{\tau\leftarrow p} \\ 1, u_{v_{i,p}} = 1 \text{ or } \sum\limits_{a \in \mathbf{A_{j,\tau}}} u_{v_{ai,p}} > 1 (v_{a,\tau}, v_{ai,p}) = e^{a\leftarrow ai}_{\tau\leftarrow p} \end{cases} \quad (2)$$

where $v_{i,p}$ is the coupled DPN node of $v_{j,\tau}$. $v_{aj,\tau} \in \mathbf{A_{j,\tau}}$ denotes the adjacent TPN node of $v_{j,t}$, and $v_{ai,p}$ is the coupled DPN node of $v_{aj,\tau}$. If the DPN node $v_{i,p}$ and any $v_{ai,p}$ fail, node $v_{j,\tau}$ breaks down due to the supply interruption from DPN and insufficient supporting capacity of $v_{aj,\tau}$.

The status $u_{e_{k,m}}$ of MN link $e_{k,m}$ is determined by its coupled TPN nodes. If all the coupled TPN nodes $v_{j,\tau} \in \mathbf{V_{j,\tau}}$ fail, the link fails.

$$u_{e_{k,m}} = \begin{cases} 0, \sum\limits_{v_{j,\tau} \in \mathbf{V_{j,\tau}}} u_{v_{j,\tau}} = 0 \\ 1, \sum\limits_{v_{j,\tau} \in \mathbf{V_{j,\tau}}} u_{v_{j,\tau}} > 0 \end{cases} (e_{k,m}, v_{j,\tau}) \in \mathbf{E}^{k\leftarrow j}_{m\leftarrow\tau} \quad (3)$$

B. Metro-Road Interdependent Network

1) Topological Interdependence: Considering the complementary relationship between RTN($\mathbf{V_R}, \mathbf{E_R}$) and MN in urban transportation, we assume each MN node has a complementary RTN node according to the geographical proximity (i.e., one-to-one coupling) which is denoted as the interdependent edge $e^{m\leftarrow r}_{j\leftarrow i} = (v_{j,m}, v_{i,r})$. The bi-level interdependent network is illustrated in Fig.5

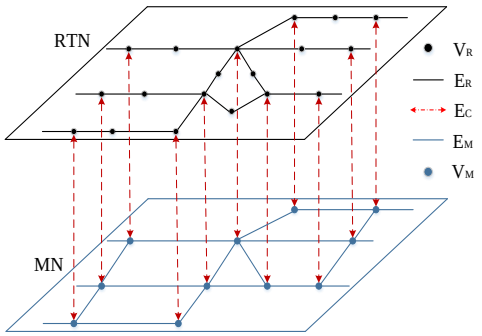

Fig. 5. The graph of MN-RTN bi-layer interdependent network

2) Functional Interdependence: The failed load of MN can be redistributed within MN through inner-layer paths or redistributed in RTN via coupled links using inter-layer paths. The former relies on the locomotive running within the electrified catenary interval with turn-back stations, while the latter depends on EB bridging routes covering the failed MN routes, as shown in Fig.6. The MN routes $\langle v_{m1}, v_{m2} \rangle$, $\langle v_{m2}, v_{m3} \rangle$, $\langle v_{m4}, v_{m5} \rangle$ are inactive due to power outage. In response, four bridging routes $R_b = \{i_{b1}, i_{b2}, i_{b3}, i_{b4}\}$ are designed to accommodate the demand of the original routes $D_f = \{D_{f1}, D_{f2}, D_{f3}, D_{f4}\}$ correspondingly.

Travelers affected by failed MN routes $r \in \mathbf{R^{out,t}_m}$ can choose inner-layer transfer routes $\mathbf{R^{r,t}_m}$ and EB bridging routes $\mathbf{R^{r,t}_b}$. The travel demand assignment considers both travel distance and travel time. The former is denoted by the number of

stations num_k of route *k* passing through, and the latter $time_k$ of route *k* is calculated by specific functions: the Davidson function for MN and BPR function for RTN [30]. The travel demand assignment of route *r* is shown as follow:

$$\begin{cases} DT_k = \frac{1/num_k - 1/num_k^{\max}}{1/num_k^{\min} - 1/num_k^{\max}} \\ time_k = \sum_{e \in \mathbf{A_k^s}} t(x_e^t) \\ TT_k = \frac{1/time_k - 1/time_k^{\max}}{1/time_k^{\min} - 1/time_k^{\max}} \\ V_k = DT_k + TT_k \\ P_k = \exp(\kappa V_k)/\sum \exp(\kappa V_i) \\ D_k^t = P_k D_{f_r}^t \end{cases}, \forall k \in \mathbf{R_b^{r,t}} \cup \mathbf{R_m^{r,t}} \quad (4)$$

where $\mathbf{A_k^e}$ is the link set related to route *k*. V_k is the utility value of route *k*, affecting the probability of being chosen by travelers, which is calculated by the normalized travel distance DT_k and travel time TT_k. P_k, D_t^k represent the chosen probability and assigned demand of route *k*, where κ is a parameter and $D_{f_r}^t$ is the travel demand of original route *r*. The calculation method of $t(x_e)$ is as follows:

$$t(x_e) = \begin{cases} t_e^0 \left[1 + J \cdot x_e/(C_e - x_e)\right], \forall e \in \mathbf{E_M} \\ t_e^0 \left[1 + \rho_{be}(x_e/c_e)^{\sigma_{be}}\right], \forall e \in \mathbf{E_R} \end{cases} \quad (5)$$

where t_e^0 and c_e are the free travel time and capacity of link *e*. C_e, x_e^t are the maximum capacity and traffic flow of link *e*. We set $\rho_{be} = 0.15$, $\sigma_{be} = 4$, $J = 0.25$ referred to [1] and [30].

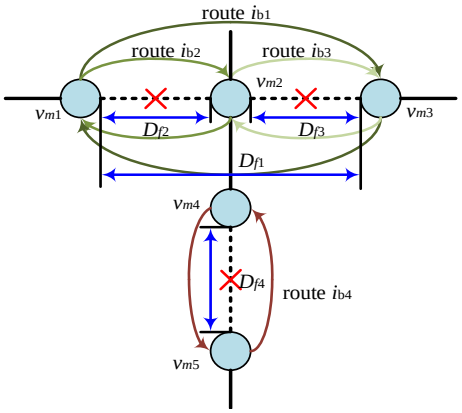

Fig. 6. The EB bridging and alternative routes for metro disruptions

C. Electric-Road Interdependent Network

1) Topological Interdependence: In RTN, the location selection of FCS considers their accessibility to nearby 10kV substations of DPN.

2) Functional Interdependence: The traffic flow of RTN affects the travel time of RC to the fault position of DPN, and the charge and discharge power of EB determines the net nodal power at FCS of DPN. These two interdependence are modeled as follows:

$$T_{(s_i,s_j)}^{travel} = \sum t(x_e), \forall e \in Path_{(s_i,s_j)} \quad (6)$$

$$P_{i_c} = \sum\nolimits_{m \in \mathbf{B}} \left(p_m^{i_c,\mathrm{dch}} - p_m^{i_c,\mathrm{ch}}\right) \forall, i_c \in \mathbf{V_P^C} \quad (7)$$

Eq. (6) formulates $T_{(s_i,s_j)}^{travel}$, and $p_m^{i_c,ch}$, $p_m^{i_c,dch}$ are the charging and discharging power of EB $m \in \mathbf{B}$ at FCS i_c in (7).

IV. Modeling of EB Route Schedule

The EBSP model is designed to allocate available EBs to meet the demands of public transit, bridging service, and power supply, defined as the original trip, bridging trip, and charge-discharge trip, respectively. As a result, a spatiotemporal network-based EPSP model is constructed, where the trips are regarded as nodes, and the transfer among them are regarded as arcs.

A. Formulation of Spatial-Temporal Network

1) Definitions of nodes and arcs: The extreme event starts at moment t_0 and divides EBs into two groups: 1) $\mathbf{B_s}$ representing the spared ones located in the depot, 2) $\mathbf{B_w}$ representing the running ones on the original routes. Three nodes and arcs are defined as follows:

- The Original Trip $\mathbf{T_o}$: Denoted by $n_m = \{t, i_o\}$, where $m \in \mathbf{B_w}$, $t \in \mathbf{T_{time}}$, $i_o \in \mathbf{R_o}$. This indicates that the EB *m* is assigned to trip n_m, departing at *t* and traveling on the original route i_o.
- The Bridging Trip $\mathbf{T_b}$: Denoted by $n_m = \{t, i_b\}$, where $m \in \mathbf{B_w} \cup \mathbf{B_s}$, $t \in \mathbf{T_{time}}$, $i_b \in \mathbf{R_b}$. This implies that the EB *m* is assigned to trip n_m, departing at *t* and traveling on the original route i_b.
- The Charge-Discharge Trip $\mathbf{T_c}$: Denoted by $n_m = \{t, i_c\}$, where $m \in \mathbf{B_w} \cup \mathbf{B_s}$, $t \in \mathbf{T_{time}}$, $i_c \in \mathbf{V_P^c}$. This indicates that the EB *m* is assigned to trip n_m, arriving at FCS i_c at *t* and staying for one time interval $\triangle T$.
- The Source Arc: Denoted by $arc = \langle o, n \rangle$, where $o \in \mathbf{O}$, $n \in \mathbf{T}$. This means that the EB *m* is assigned to trip *n* departing from depot *o*.
- The Moving Arc: Denoted by $arc = \langle n^1, n^2 \rangle$, where $n^1, n^2 \in \mathbf{T}$. This means that the EB *m* transfer from trip n^1 to n^2.
- The Sink Arc: Denoted by $arc = \langle n, o \rangle$, where $o \in \mathbf{O}$, $n \in \mathbf{T}$. This means that the EB *m* returns to depot *o* after completing trip *n*.

2) Spatial-Temporal Network: The spatial-temporal network is modeled as a weighted graph $g = \{\mathbf{T}, \mathbf{A}, \mathbf{W}\}$, which is illustrated in Fig.7. The horizontal axis denotes the departure time of trip $\mathbf{T_o}$, $\mathbf{T_b}$ and the arrival time of trip $\mathbf{T_c}$, while the vertical axis denotes the route of trip $\mathbf{T_o}$, $\mathbf{T_b}$ and the destination FCS of trip $\mathbf{T_c}$. To ensure the network flow conservation and continuity, the following assumptions are made:

- Each bus $m \in \mathbf{B_s}$ will return to the depot after completing its service.
- Each bus $m \in \mathbf{B_w}$ assigned to trip $\mathbf{T_o}$ must originate from the one running on its original route i_o at t_0.
- A bus cannot switch to another trip midway without completing the ongoing one.

B. EB Route Schedule Model with Service Trips

The schedule route of EB *m* is represented as a sequence of nodes and arcs. Hence, two binary variables α_m^n, $x_m^{n^1 n^2}$ are defined to describe the status of EB. If EB *m* is assigned to trip *n*, then $\alpha_m^n = 1$. Similarly, if EB *m* is assigned through $arc = \langle n^1, n^2 \rangle$, then $x_m^{n^1 n^2} = 1$.

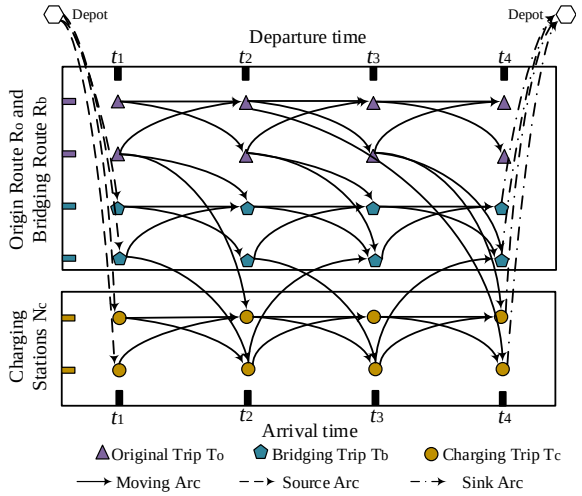

Fig. 7. The illustration of the EB spatial-temporal network

1) Constraints on Trips:

$$\sum\nolimits_m C_m \alpha_m^n \geq D_{i_o}, \forall n = \{t, i_o\} \in \mathbf{T_o}, m \in \mathbf{B_w} \quad (8)$$

$$\theta D_{i_b}^t \leq \sum\nolimits_m C_m \alpha_m^n \leq D_{i_b}^t, \forall n = \{t, i_b\} \in \mathbf{T_b}, m \in \mathbf{B_w} \cup \mathbf{B_s} \quad (9)$$

$$\sum\nolimits_m \alpha_m^n \leq C_{i_c}, \ \forall n = \{t, i_c\} \in \mathbf{T_c}, m \in \mathbf{B_w} \cup \mathbf{B_s} \quad (10)$$

$$\sum\nolimits_m \alpha_m^n \leq N_B, \ \forall n \in \mathbf{T}, m \in \mathbf{B_w} \cup \mathbf{B_s} \quad (11)$$

Constraint (8) ensures sufficient EBs for the original trip $\mathbf{T_o}$ to meet the minimum transit demand D_{i_o} of each route i_o. C_m is the passenger capacity of EB *m*. Constraint (9) ensures adequate EBs for the bridging trip $\mathbf{T_b}$ to meet the demand of bridging route i_b, where $\theta \in [0, 1]$ is the tolerance coefficient. Constraint (10) limits the number of EBs assigned for charge-discharge trip $\mathbf{T_c}$ to the capacity C_{i_c} of FCS i_c. Constraint (11) restricts the number of EBs for all service trips within the maximum number.

2) Constraints on Flow Conservation: In the spatial-temporal network, nodes are connected to each other through arcs, with node *n* being the end point of its precedent node n^1 and the start point of its succeeding node n^2. Hence, the following constraints are established to ensure that the inflow of a node must equal its outflow.

$$\sum_{\langle n^1 n \rangle \in \mathbf{A_n^e}} x_m^{n^1 n} = \sum_{\langle n n^2 \rangle \in \mathbf{A_n^s}} x_m^{n n^2} = \alpha_m^n, \forall n \in \mathbf{T_b} \cup \mathbf{T_c}, m \in \mathbf{B_s} \quad (12)$$

$$\sum_{\langle n^1 n \rangle \in \mathbf{A_n^e}} x_m^{n^1 n} = \sum_{\langle n n^2 \rangle \in \mathbf{A_n^s}} x_m^{n n^2} = \alpha_m^n, \ \forall n, m \in \mathbf{B_w} \quad (13)$$

$$\sum_n x_m^{on} = \sum_n x_m^{no} \leq 1, \ \forall n \in \mathbf{T_b} \cup \mathbf{T_c}, m \in \mathbf{B_s} \quad (14)$$

$$\sum_n x_m^{on} = \sum_n x_m^{no} = 0, \ \forall n, m \in \mathbf{B_w} \quad (15)$$

where $\mathbf{A_n^e}$ and $\mathbf{A_n^s}$ are the arc sets ending at node *n* and starting at node *n*. Constraints (12)-(13) enforce inflow and one outflow for EB *m* assigned to trip *n* from $\mathbf{B_s}$ and $\mathbf{B_w}$, respectively. Constraint (14) ensures that each EB $m \in \mathbf{B_w}$ has only one source arc and one sink arc, signifying its return to the depot after trips completion. Constraint (15) indicates that EB $m \in \mathbf{B_s}$ has neither source arc nor sink arc as it does not depart from the depot.

3) Constraints on the relations between nodes and arcs: The variable $x_m^{n^1 n^2}$ is related to $\alpha_m^{n^1}$ and $\alpha_m^{n^2}$, representing the status of head node and tail node of the arc $\langle n^1, n^2 \rangle \in \mathbf{A}$, respectively.

$$x_m^{n^1 n^2} \leq \alpha_m^{n^1} \alpha_m^{n^2} \forall n^1, \forall n^2 \in \mathbf{T} \quad (16)$$

A constraint is introduced to restrict the assignment of trips to EB, ensuring there is no time overlap, considering their respective duration and the transfer time between them.

$$\begin{cases} t_{n^1}^e + t_{n_1^1}^{n^2} \leq t_{n^2}^b, n^2 \in \mathbf{T_b} \cup \mathbf{T_o} \\ t_{n^1}^e + t_{n^1}^{n^2} = t_{n^2}^b, n^2 \in \mathbf{T_c} \end{cases} \forall n^1 \in \mathbf{T} \quad (17)$$

where $t_{n^1}^e$, $t_{n^2}^b$ and $t_{n^1}^{n^2}$ are the end time of trip n^1, start time of trip n^2, and the transfer time between them, respectively.

4) Operation Constraints of EB: When EB *m* is serving trip $\mathbf{T_c}$, it can exchange electricity with DPN through FCS i_c while consuming energy when serving trip $\mathbf{T_o}$ and $\mathbf{T_b}$. Hence, the constraints on the energy change of each EB are as follows:

$$0 \leq p_{mt}^{n,\mathrm{dch}} \leq \beta_m^{n,\mathrm{dch}} \overline{p_m^{\mathrm{dch}}}, \ \forall n = \{t, i_c\} \in \mathbf{T_c} \quad (18)$$

$$0 \leq p_{mt}^{n,\mathrm{ch}} \leq \beta_m^{n,\mathrm{ch}} \overline{p_m^{\mathrm{ch}}}, \ \forall n = \{t, i_c\} \in \mathbf{T_c} \quad (19)$$

$$\beta_m^{n,\mathrm{dch}} + \beta_m^{n,\mathrm{ch}} \leq \alpha_m^n, \ \forall n = \{t, i_c\} \in \mathbf{T_c} \quad (20)$$

$$\underline{soc_m} \leq soc_m^{t_i} \leq \overline{soc_m}, \ \forall t_i \in \mathbf{T_{time}} \quad (21)$$

$$soc_m^{t_{i+1}} = soc_m^{t_i} + \Delta soc_m^t, \ \forall t_i \in \mathbf{T_{time}} \quad (22)$$

$$\begin{aligned} \Delta soc_m^t = & \frac{\Delta T}{C_m} \left(\eta_m^{\mathrm{ch}} \sum_{n \in \mathbf{T_c}} p_{mt}^{n,\mathrm{ch}} - \eta_m^{\mathrm{dch}^{-1}} \sum_{n \in \mathbf{T_c}} p_{mt}^{n,\mathrm{dch}} \right) \\ & - \frac{\Delta T}{C_m} \left(\sum_{n \in \mathbf{T_o} \cup \mathbf{T_b}} \alpha_m^n p_m^n + \sum_{\langle n^1 n^2 \rangle \in \mathbf{A}} x_m^{n^1 n^2} p_m^{n^1 n^2} \right) \end{aligned} \quad (23)$$

Constraints (18)-(20) describe the charging and discharging behavior of EB *m*, where $\overline{p_m^{\mathrm{ch}}}$, $\overline{p_m^{\mathrm{dch}}}$ are their respective upper bounds. In constraint (21), the SOC bound of EB *m* at *t* is bounded to the interval $[\underline{soc_m}, \overline{soc_m}]$. Eqs. (22)-(23) express the change of SOC $soc_m^{t_i}$, where the SOC variation Δsoc_m^t over a time interval depends on three terms: energy exchange in trip $\mathbf{T_c}$, energy consumption in trips $\mathbf{T_o}$ and $\mathbf{T_b}$, and the energy consumption during transfers among these three trips. p_m^n, $p_m^{n^1 n^2}$ are the power consumption during trip *n* and arc $\langle n^1, n^2 \rangle$, and the performing time should satisfy the following conditions:

$$t_n^b \leq t, t_n^e \geq t + \Delta T, \ \forall n \in \mathbf{T_b} \cup \mathbf{T_o} \quad (24)$$

$$t_{n^1}^b \leq t, t_{n^2}^e \geq t + \Delta T, \ \forall \langle n^1, n^2 \rangle \in \mathbf{A} \quad (25)$$

V. DPN Restoration Model with EB

A. Objective

The objective function of DPN restoration model is designed to minimize the time cost of lost load considering the unsatisfied coupling MN traffic demand during the recovery.

$$\min \sum_t \Delta T \left[\sum_{i \in \mathbf{V_P} / \mathbf{V_P^{couple}}} \varpi_1^{i,t} \Delta P_{i,L}^t + \sum_{i \in \mathbf{V_P^{couple}}} \varpi_2^{i,t} \Delta P_{i,L}^t \right] \quad (26)$$

$$\begin{cases} \varpi_1^{i,t} = \varpi_1 \exp\left[\delta_1(1+t/T)\right], \forall i \in \mathbf{V_P}/\mathbf{V_P^{couple}} \\ \varpi_2^{i,t} = \varpi_2 \exp\left[\delta_1(1+t/T)\right](1+\beta_i^t), \forall i \in \mathbf{V_P^{couple}} \end{cases} \quad (27)$$

$$\beta_i^t = \delta_2 \sum_{i_b \in \mathbf{R_b^t}} (D_{i_b}^t - C_m \sum_{m \in \mathbf{B}} \alpha_m^n) \Big/ \sum_{i_b \in \mathbf{R_b^t}} D_{i_b}^t, \forall n = \{t, i_b\} \quad (28)$$

in function (26), DPN nodes $\mathbf{V_P}$ are categorized into two sets: $\mathbf{V_P^{couple}}$ and $\mathbf{V_P}/\mathbf{V_P^{couple}}$, denoting the nodal load coupled with and without MN traffic demand. $\Delta P_{i,L}^t$ is nodal load loss. Eq. (27) formulates time cost functions $\varpi_1^{i,t}$, $\varpi_2^{i,t}$ for load loss of $\mathbf{V_P}/\mathbf{V_P^{couple}}$ and $\mathbf{V_P^{couple}}$, respectively, and ϖ_1, ϖ_2 denote the importance degree of nodal load. β_i^t in Eq. (28) is the rate of unsatisfied traffic demand due to nodal load loss. Penalty coefficients δ_1 and δ_2 are set to 2 and 10 in this paper.

B. Network Reconfiguration

After outage, DPN reconfigures into multiple isolated islands that functioning as MGs, aiming to minimize load loss. The MG topology with a single source is typically radial, which may change during restoration. To maintain radial topology, we employ a directed graph-based method in [17]. Initially, a virtual node v_0 only connected to source nodes of the original network via virtual lines, is introduced to form a virtual network, illustrated in Fig.8. The links among them are represented as virtual lines. Subsequently, v_0 generates virtual power transmitted through virtual lines to fullfill the virtual load f_i^{load} of each DPN node, denoted by f_{ij}^t, where $f_i^{load} = 1$. The Constraints are as follows:

$$s_{ij}^t = s_{ij,d}^t + s_{ji,r}^t, \forall (ij) \in \mathbf{E_P} \quad (29)$$

$$s_{ij}^t \le u_{ij}^t, \forall (ij) \in \mathbf{E_P} \quad (30)$$

$$s_{j0,r}^t = 0, \forall j \in \mathbf{V_P^C} \cup \mathbf{V_P^M} \cup \mathbf{V_P^D} \quad (31)$$

$$s_{0j,d}^t = 1, \forall j \in \mathbf{V_P^S}(t) \quad (32)$$

$$s_{0j,d}^t = 0, \forall j \in \left\{\mathbf{V_P^C} \cup \mathbf{V_P^M} \cup \mathbf{V_P^D}\right\} \setminus \mathbf{V_P^S}(t) \quad (33)$$

$$\sum_{i \in \mathbf{A_k}} s_{ik,d}^t + \sum_{j \in \mathbf{A_k}} s_{jk,r}^t \le 1, \forall k \in \mathbf{V_P} \quad (34)$$

$$\sum_{i \in \mathbf{A_k}} s_{ik,d}^t + \sum_{j \in \mathbf{A_k}} s_{jk,r}^t \ge z_k^t, \forall k \in \mathbf{V_P} \quad (35)$$

$$s_{ij}^t - 1 \le z_i^t - z_j^t \le 1 - s_{ij}^t, \forall i,j \in \mathbf{V_P} \quad (36)$$

$$-z_i^t f_i^{load} = \sum_{j \in \mathbf{A_i}} f_{ij}^t, \forall i \in \mathbf{V_P} \quad (37)$$

$$-s_{ij}^t \cdot N_P \le f_{ij}^t \le -s_{ij}^t \cdot N_P, \forall (ij) \in \mathbf{E_P} \cup \mathbf{E_{VP}} \quad (38)$$

$$z_i^t = 1, \forall i \in \mathbf{V_P^S}(t) \quad (39)$$

$$z_i^t \le 1, \forall i \in \mathbf{V_P} \setminus \mathbf{V_P^S}(t) \quad (40)$$

Constraint (29) relates the state of line (ij) to its power flow direction. Binary variables $s_{ij,d}^t$ and $s_{ji,r}^t$ denote power flow direction, where $s_{ij,d}^t = 1$ if power flows from *i* to *j* at t and $s_{ji,r}^t = 1$ if power flows in reverse. Constraint (30) allows line (ij) closure only if it is repaired or undamaged ($u_{ij}^t = 1$). Constraints (31)-(33) ensure virtual power only flows from v_0 to the outputting source nodes $\mathbf{V_P^S(t)}$ at *t*. Constraints (34)-(35) ensure each DPN node *k* powered by only one parent node, where $\mathbf{A_k}$ is the set of adjacent nodes. Constraint (36) maintains line state consistency with bilateral node states. Constraint (37)-(38) balance node virtual power and set line virtual flow bounds ($\mathbf{E_{VP}}$ is the set of virtual lines). Constraints (39)-(40) limit outputting source node states and other load node states.

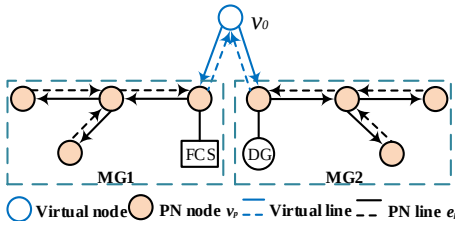

Fig. 8. The directed graph of virtual network

C. Repair Crew

$$T_{s_j}^{ch} = T_{s_j}^{re} + T_{(s_i,s_j)}^{travel}, \forall s_j \in \mathbf{S_P}, s_i \in \{\mathbf{S_P} \cup \mathbf{S_o}\} \quad (41)$$

$$\sum_{t \in \mathbf{T_{time}}} \chi_{c_i,s_j}^t = T_{s_j}^{ch}, \forall c_i \in \mathbf{C_{re}}, s_j \in \mathbf{S_P} \quad (42)$$

$$-M(1-q_{s_j}^t) + T_{s_j}^{ch} \le \sum_{\tau=t-T_{s_j}^{re}}^{t} \chi_{c_i,s_j}^{\tau} \le M(1-q_{s_j}^t) + T_{s_j}^{ch}, \forall t \in \mathbf{T_{time}} \quad (43)$$

$$\sum_{c_i \in \mathbf{C_{re}}} \sum_{s_j \in \mathbf{S_P}} \chi_{c_i,s_j}^t \le N_{re}, \forall t \in \mathbf{T_{time}} \quad (44)$$

$$u_{s_j}^t = q_{s_j}^t, \forall s_j \in \mathbf{S_P}, t \in \mathbf{T_{time}} \quad (45)$$

Constraint (41) defines the recovery time $T_{s_j}^{ch}$ of fault $s_j \in \mathbf{S_P}$ as the sum of repair time $T_{s_j}^{re}$ and the minimum travel time $T_{(s_i,s_j)}^{travel}$ for RC to reach s_j, where $\mathbf{S_o}$ denotes its depot. Constraints (42)-(43) ensure that crew $c_i \in \mathbf{C_{re}}$ is assigned to the failed component continuously until its recovery. Constraint (44) limits the number of crews with repair assignments to the total number N_{re} at *t*. Constraint (45) describes that s_j returns to normal upon its recovery at *t*.

D. Coupling Components in ETIN

1) MN Link Constraints: We define $\mathbf{E_M^{out}}$ as the initial set of failed MN links due to power off that will recover with the restoration of DPN. The coupling constraints are added as follows.

$$u_{e_{k,m}}^t = 1 - \prod_{v_{j,\tau} \in \mathbf{V_T}} (1 - u_{v_{j,\tau}}^t), \forall (e_{k,m}, v_{j,\tau}) \in \mathbf{E}_{m \leftarrow \tau}^{k \leftarrow j}, e_{k,m} \in \mathbf{E_M^{out}} \quad (46)$$

$$u_{v_{j,\tau}}^t = 1 - (1 - u_{v_{i,p}}^t)(1 - \prod_{a \in \mathbf{A_{j,\tau}}} u_{v_{ai,p}}^t), \forall (v_{j,\tau}, v_{i,p}) = e_{\tau \leftarrow p}^{j \leftarrow i} \quad (47)$$

where $u_{e_{k,m}}^t$, $u_{v_{j,\tau}}^t$ and $u_{v_{i,p}}^t$ denoting the state of MN link $e_{k,m}$, TPN node $v_{j,\tau}$ and DPN node $v_{i,p}$ that are coupled with each other. $u_{v_{ai,p}}^t$ denotes the state of DPN node $v_{ai,p}$ that is coupled with the adjacent TPN node $v_{aj,\tau}$ of $v_{j,\tau}$.

In ETIN, each MN link is supplied by two TPN nodes with two neighboring nodes, and each TPN node is coupled with one DPN node. We introduce binary variables

$\kappa_1 = 1 - u^t_{v_{j1,\tau}}$, $\kappa_2 = 1 - u_{v_{j2,\tau}}$, $\kappa_3 = \kappa_1\kappa_2$, $\kappa_4 = 1 - u_{v_{i,p}}$, $\kappa_5 = 1 - u^t_{v_{ai1,p}} u^t_{v_{ai2,p}}$, $\kappa_6 = \kappa_4\kappa_5$, and Eqs. (46)-(47) can be substituted with the following expressions (48)-(49)

$$u^t_{e_{k,m}} = 1 - \kappa_3 \tag{48}$$

$$u^t_{v_{j,\tau}} = 1 - \kappa_6 \tag{49}$$

where κ_3, κ_5 and κ_6 can be equivalently linearized by satisfying the following constraints:

$$\begin{cases}\kappa_3 \le \kappa_1, \kappa_3 \le \kappa_2\\ \kappa_3 \ge \kappa_1 + \kappa_2 - 1\end{cases}\begin{cases}\kappa_5 \le u^t_{v_{ai1,p}}, \kappa_5 \le u^t_{v_{ai2,p}}\\ \kappa_5 \ge u^t_{v_{ai1,p}} + u^t_{v_{ai2,p}} - 1\end{cases}\begin{cases}\kappa_6 \le \kappa_4, \kappa_6 \le \kappa_5\\ \kappa_6 \ge \kappa_4 + \kappa_5 - 1\end{cases} \tag{50}$$

where Eq. (48) indicates that MN link $e_{k,m}$ can operate if either coupled TPN node $v_{j,\tau}$ works at *t*. Eq. (49) indicates that node $v_{j,\tau}$ can be powered under two cases: 1) its coupled DPN node $v_{i,p}$ is working at *t*, 2) both DPN nodes $v_{ai1,p}$ and $v_{ai2,p}$, coupled with its adjacent TPN nodes $v_{a1,\tau}$ and $v_{a2,\tau}$ respectively, are operational at *t*.

2) Bridging Route Constraints: We introduce a binary variable $u^t_{i_b}$ to denote the existence of bridging route i_b. During the restoration of DPN, the recovery of certain failed MN links may affect the state of the coupling route i_b.

$$u^t_{i_b} = \prod (1 - a^{i_b}_{e,m} u^t_{e_{k,m}}), \forall i_b \in \mathbf{R_b}, e_{k,m} \in \mathbf{E^{out}_M}, a^{i_b}_{e,m} \in \mathbf{A^{i_b}_{e,m}} \tag{51}$$

$$D^t_{i_b} = D_{i_b} u^t_{i_b},\ \forall i_b \in \mathbf{R_b} \tag{52}$$

where $\mathbf{A^{i_b}_{e,m}}$ is the adjacent matrix of MN links and bridging routes. $a^{i_b}_{e,m} = 1$ if route i_b traverses link $e_{k,m}$. The linearization method is as explained in the above section.

E. DPN Operation

The LinDistFlow model in [31] is employed to model the operation of DPN.

1) Nodal Power Balance Constraints:

$$P^t_{i,G} - P^t_{i,L} = \sum\nolimits_{(ij)\in\mathbf{E_P}} P^t_{ij},\ \forall i, t \tag{53}$$

$$Q^t_{i,G} - Q^t_{i,L} = \sum\nolimits_{(ij)\in\mathbf{E_P}} Q^t_{ij},\ \forall i, t \tag{54}$$

$$0 \le P^t_{i,G} \le P^M_{i,G},\ \forall i \in \mathbf{V^M_P}, t \tag{55}$$

$$0 \le Q^t_{i,G} \le Q^M_{i,G},\ \forall i \in \mathbf{V^M_P}, t \tag{56}$$

$$\underline{P_{i,G}} \le P^t_{i,G} \le \overline{P_{i,G}},\ \forall i \in \mathbf{V^D_P}, t \tag{57}$$

$$\underline{Q_{i,G}} \le Q^t_{i,G} \le \overline{Q_{i,G}},\ \forall i \in \mathbf{V^D_P}, t \tag{58}$$

$$P^t_{i_c,G} = \sum\nolimits_{m\in\mathbf{B}} \left(p^{n,\mathrm{dch}}_{mt} - p^{n,\mathrm{ch}}_{mt}\right), \forall n \in \mathbf{T_c}, i_c \in \mathbf{V^C_P}, t \tag{59}$$

$$\underline{Q_{i_c,G}} \le Q^t_{i_c,G} \le \overline{Q_{i_c,G}},\ \forall i_c \in \mathbf{V^C_P}, t \tag{60}$$

where $P^t_{i,L}$, $Q^t_{i,L}$ are the active and reactive load of node *i* at *t*, while $P^t_{i,G}$, $Q^t_{i,G}$ are the active and reactive output power of node *i* at *t*. P^t_{ij}, Q^t_{ij} are the active and reactive power flow on line (ij) at *t*. Constraints (55)-(56), (57)-(58) and (59)-(60) restrict the output of source nodes connected to the main grid, DG, and FCS respectively.

2) Load Restoration Constraints:

$$0 \le P^t_{i,L} \le z^t_i \overline{P_{i,L}},\ \forall i, t \tag{61}$$

$$Q^t_{i,L} = \tan(\cos^{-1}\phi_i) P^t_{i,L},\ \forall i, t \tag{62}$$

$$P^t_{i,L} \le P^{t+1}_{i,L},\ \forall i \in \mathbf{V^{couple}_P}, t \ge t_1 \tag{63}$$

Constraint (61) correlates load restoration with node status, and ϕ_i is the power factor angle in Eq. (62). Constraint (63) indicates that the recovered load coupled with MN traffic demand will not be shut down in the following process.

3) Power Flow Constraints:

$$-s^t_{ij}\overline{S_{ij}} \le P^t_{ij} \le s^t_{ij}\overline{S_{ij}},\ \forall (ij) \in \mathbf{E_P}, t \tag{64}$$

$$-s^t_{ij}\overline{S_{ij}} \le Q^t_{ij} \le s^t_{ij}\overline{S_{ij}},\ \forall (ij) \in \mathbf{E_P}, t \tag{65}$$

$$-\sqrt{2}s^t_{ij}\overline{S_{ij}} \le P^t_{ij} + Q^t_{ij} \le \sqrt{2}s^t_{ij}\overline{S_{ij}},\ \forall (ij) \in \mathbf{E_P}, t \tag{66}$$

$$-\sqrt{2}s^t_{ij}\overline{S_{ij}} \le P^t_{ij} - Q^t_{ij} \le \sqrt{2}s^t_{ij}\overline{S_{ij}},\ \forall (ij) \in \mathbf{E_P}, t \tag{67}$$

$$V^t_i = V_0,\ \forall i \in \mathbf{V^S_P}(t) \tag{68}$$

$$u_i\underline{V_i} \le V^t_i \le u_i\overline{V_i},\ \forall i \in \mathbf{V_P} \backslash \mathbf{V^S_P}(t) \tag{69}$$

$$V^t_i - V^t_j \le M(1 - s^t_{ij}) + \left(R_{ij}P^t_{ij} + X_{ij}Q^t_{ij}\right)/V_0,\ \forall (ij), t \tag{70}$$

$$V^t_i - V^t_j \ge M(s^t_{ij} - 1) + \left(R_{ij}P^t_{ij} + X_{ij}Q^t_{ij}\right)/V_0,\ \forall (ij), t \tag{71}$$

Inequations (64)-(67) are the linearized form of lines transmission capacity constraints, where $\overline{S_{ij}}$ is the maximum apparent power. Constraints (68)-(69) stipulate the voltage of outputting sources nodes and other nodes. Constraints (70)-(71) describe the relation between node voltage and power flow.

F. Optimization Problem Formulation

The DPN restoration problem is formulated as an MILP model that is summarized as follows:

Objective function: (26)-(28)

Constraints are classified into following five groups:

1) EBSP: (8)-(11), (12)-(15), (16)-(17), (18)-(25).

2) Network Reconfiguration: (29)-(40).

3) Schedule of Repair Crews: (41)-(45).

4) State of Coupling Components in ETIN: (48)-(52).

5) LinDistFlow for DPN Operation: (53)-(71).

G. A Fast Restoration Algorithm based on AIF Model

The proposed MILP model can be compactly expressed as:

$$\min \sum_{\forall t}\sum_{\forall i} \varpi_{i,t} \Delta P^t_{i,L} \tag{72}$$

$$s.t. \mathbf{I}(\mathbf{b}_\mathrm{p}, \mathbf{b}_\mathrm{b}, \mathbf{b}_\mathrm{o}, \mathbf{c}_\mathrm{p}, \mathbf{c}_\mathrm{b}) \le 0, \mathbf{E}(\mathbf{b}_\mathrm{p}, \mathbf{b}_\mathrm{b}, \mathbf{b}_\mathrm{o}, \mathbf{c}_\mathrm{p}, \mathbf{c}_\mathrm{b}) = 0 \tag{73}$$

$$\mathbf{b} = [\mathbf{b}_\mathrm{p}, \mathbf{b}_\mathrm{b}, \mathbf{b}_\mathrm{o}] \in \{0,1\}, \mathbf{c} = [\mathbf{c}_\mathrm{p}, \mathbf{c}_\mathrm{b}] \in [\mathbf{c}_\mathrm{min}, \mathbf{c}_\mathrm{max}] \tag{74}$$

where $\{\mathbf{b}_\mathrm{p}, \mathbf{c}_\mathrm{p}\}$ and $\{\mathbf{b}_\mathrm{b}, \mathbf{c}_\mathrm{b}\}$ denote integer and continuous variables associated with DPN operation including network reconfiguration and EB schedule, respectively, whereas $\mathbf{b}_\mathrm{o}$ denotes other integer variables associated with RC schedule and states constraints of coupling components in ETIN. $\mathbf{I}$ and $\mathbf{E}$ represent inequality and equality constraints, respectively. To accelerate computation, the original model can be transformed into an AIF model with the auxiliary induce function, with solution accuracy guarantees [32]-[33]. Compared with the constructed AIF in [34], where only integer variables denoting the power line status were considered. We design two AIFs for integer variables $\mathbf{b}_\mathrm{p}$ and $\mathbf{b}_\mathrm{b}$, respectively, to further improve the solving efficiency. Specifically, $\mathbf{b}_\mathrm{p} = \left\{s_{ij}, s_{ij,d}, s_{ij,r}, z_i, q_{s_j}\right\}$

and $\mathbf{b}_{\mathrm{b}}=\left\{\alpha_m^n, x_m^{n^1 n^2}\right\}$. The AIF model adjusts coefficients for integer variables in its objective function based on the insights from the relaxation solution of the original MILP, while keeping constraints unchanged, succinctly presented in (75)-(76).

$$\min\left(\sum_{\forall t}\sum_{\forall i}\varpi_{i,t}\Delta P_{i,L}^{t}+\sum_{\forall t}\sum_{\forall p}\sigma_{p,t}b_{p,t}+\sum_{\forall t}\sum_{\forall b}\sigma_{b,t}b_{b,t}\right) \tag{75}$$

$$s.t.\mathbf{I}(\mathbf{b},\mathbf{c})\leq 0,\mathbf{E}(\mathbf{b},\mathbf{c})=0,\mathbf{b}\in\{0,1\},\mathbf{c}\in[\mathbf{c}_{\min},\mathbf{c}_{\max}] \tag{76}$$

where $\sigma_{p,t}$ and $\sigma_{b,t}$ are *auxiliary induce function factor* (AIFF) of integer variables $b_{p,t}$ and $b_{b,t}$, respectively, which can be calculated by:

$$\sigma_{p,t}=\varepsilon_p\times\left(-\widetilde{b_{p,t}}+\frac{1}{N_p}\times\sum_{\forall p}\widetilde{b_{p,t}}\right) \tag{77}$$

$$\sigma_{b,t}=\varepsilon_b\times\left(-\widetilde{b_{b,t}}+\frac{1}{N_b}\times\sum_{\forall b}\widetilde{b_{b,t}}\right) \tag{78}$$

$$\widetilde{\mathbf{b}_{\mathrm{p}}}=\arg\left\{\min\sum_{\forall t}\sum_{\forall i}\varpi_{i,t}\Delta P_{i,L}^{t}\right\},s.t.0\leq\widetilde{b_{p,t}}\leq 1 \tag{79}$$

$$\widetilde{\mathbf{b}_{\mathrm{b}}}=\arg\left\{\min\sum_{\forall t}\sum_{\forall i}\varpi_{i,t}\Delta P_{i,L}^{t}\right\},s.t.0\leq\widetilde{b_{b,t}}\leq 1 \tag{80}$$

where $\widetilde{b_{p,t}}$ and $\widetilde{b_{b,t}}$ are the solutions of relaxed problems (79) and (80). In (79) and (80), only the integer variables $b_{p,t}$ and $b_{b,t}$ are linearized, respectively, while the remaining variables and constraints keep the same with (76). N_p and N_b denote the dimensions of $\mathbf{b_p}$ and $\mathbf{b_b}$, respectively. ε_p and ε_b are scaling parameter that should follow a strict criterion (81) to control the relative calculation error from the AIFF below δ, with the specified optimality gap ϕ.

$$\begin{cases}\varepsilon_p=[C_{lp}\times(\delta-\phi)]\Big/\left[N_p\times\left(\widetilde{b_{p,t}^{\max}}-\widetilde{b_{p,t}^{\min}}\right)\right]\\ \varepsilon_b=[C_{lb}\times(\delta-\phi)]\Big/\left[N_b\times\left(\widetilde{b_{b,t}^{\max}}-\widetilde{b_{b,t}^{\min}}\right)\right]\end{cases} \tag{81}$$

where C_{lp} and C_{lb} are the optimal value of problem (79) and (80), respectively. Noting that the denominator can equal zero when $\widetilde{\mathbf{b}_t}$ is either $[0,...,0]_{1\times n}$ or $[1,...,1]_{1\times n}$. In such cases, σ of $\widetilde{b_t}$ is set to a large positive number *M* if $\widetilde{\mathbf{b}_t}$ is the zero vector and to *-M* otherwise.

VI. Distributed Method for The Integrated DPN Restoration Model

Given that the post-event DPN restoration involves the coordination among different stakeholders, we propose a distributed method to solve such an integrated model. Two entities are considered: the DPN company and the EB company. The DPN has no authority to dispatch EBs while EB company cannot access the topology and operation information of the DPN. Furthermore, only limited information is exchanged between the two entities, as defined in the following subproblem formulation. It is important to note that metro operations rely on power supply from the TPN, which serves as the power load for the DPN. Metro route failures are primarily caused by power outages and can be resolved once the associated power load is restored. Hence, as a critical load of the DPN, the MN restoration is managed by the DPN company, which is incorporated into objective (26) of our original integrated model.

A. Subproblem Formulation

The proposed original integrated MILP model can be compactly expressed as:

$$\begin{aligned}\min\ &\underbrace{\sum_t\Delta T\left[\sum_{i\in\mathbf{V_P}/\mathbf{V_P^{couple}}}\varpi_1^{i,t}\Delta P_{i,L}^t+\sum_{i\in\mathbf{V_P^{couple}}}\varpi_2^{i,t}\Delta P_{i,L}^t\right]}_{F_p(\mathbf{b}_{\mathrm{p}},\mathbf{c}_{\mathrm{p}})}\\ &+\underbrace{\sum_t\Delta T\left[\sum_{\forall m}\left(\overline{soc_m}-soc_m^{t_i}\right)\right]}_{F_b(\mathbf{b}_{\mathrm{b}},\mathbf{c}_{\mathrm{b}})}\\ &subject\ to\\ &\begin{cases}\mathbf{I}(\mathbf{b}_{\mathrm{p}},\mathbf{c}_{\mathrm{p}},\mathbf{\Psi}_{\mathrm{p}})\leq 0,\mathbf{E}(\mathbf{b}_{\mathrm{p}},\mathbf{c}_{\mathrm{p}},\mathbf{\Psi}_{\mathrm{p}})=0\\ \mathbf{I}(\mathbf{b}_{\mathrm{b}},\mathbf{c}_{\mathrm{b}},\mathbf{\Psi}_{\mathrm{b}})\leq 0,\mathbf{E}(\mathbf{b}_{\mathrm{b}},\mathbf{c}_{\mathrm{b}},\mathbf{\Psi}_{\mathrm{b}})=0\\ \mathbf{\Psi}_{\mathrm{p}}=\mathbf{\Psi}_{\mathrm{b}},\mathbf{\Psi}_{\mathrm{p}}=\left\{P_{i_c,G}^t,N_{i_b}^t\right\},\mathbf{\Psi}_{\mathrm{b}}=\left\{p_{i_c}^t,n_{i_b}^t\right\}\\ \mathbf{b}_{\mathrm{p}}=\left\{s_{ij}^t,s_{ij,d}^t,s_{ji,r}^t,u_{ij}^t,\mathrm{z}_i^t,q_{s_j}^t,\chi_{c_i,s_j}^t,u_{i_b}^t\right\}\\ \mathbf{c}_{\mathrm{p}}=\left\{P_{i,G}^t,Q_{i,G}^t,P_{i,L}^t,P_{ij}^t,Q_{ij}^t,V_i^t,f_{ij}^t\right\}\\ \mathbf{b}_{\mathrm{b}}=\left\{\alpha_m^n,x_m^{n^1n^2},\beta_m^{n,\mathrm{dch}},\beta_m^{n,\mathrm{ch}}\right\}\\ \mathbf{c}_{\mathrm{b}}=\left\{p_{mt}^{n,\mathrm{dch}},p_{mt}^{n,\mathrm{ch}},soc_m^t\right\}\\ \mathbf{b}=\{\mathbf{b}_{\mathrm{p}},\mathbf{b}_{\mathrm{b}}\}\in\{0,1\},\mathbf{c}=\{\mathbf{c}_{\mathrm{p}},\mathbf{c}_{\mathrm{b}}\}\in[\mathbf{c}_{\min},\mathbf{c}_{\max}]\\ \mathbf{\Psi}=\{\mathbf{\Psi}_{\mathrm{p}},\mathbf{\Psi}_{\mathrm{b}}\}\in[\Psi_{\min},\Psi_{\max}]\end{cases}\end{aligned} \tag{82}$$

(83)

where F_p and F_b represent the benefits of DPN company and EB company, respectively. $\{\mathbf{b}_{\mathrm{p}},\mathbf{c}_{\mathrm{p}}\}$ denote integer and continuous variables associated with DPN, including network reconfiguration and operation, repair crew schedule and bridging services of affected MN routes (DPN restoration subproblem). $\{\mathbf{b}_{\mathrm{b}},\mathbf{c}_{\mathrm{b}}\}$ denote integer and continuous variables associated with EB schedules (EBSP subproblem). Similarly, $\{\mathbf{\Psi}_{\mathrm{p}},\mathbf{\Psi}_{\mathrm{b}}\}$ denote the coupled continuous variables between the DPN restoration subproblem and the EBSP subproblem. For the purpose of distributed implementation, we first introduce the DPN restoration subproblem and EBSP subproblem by augmented Lagrangian decomposition (ALD), with relaxing constraint $\mathbf{\Psi}_{\mathrm{p}}=\mathbf{\Psi}_{\mathrm{b}}$, i.e., $P_{i_c,G}^t=p_{i_c}^t$, $N_{i_b}^t=n_{i_b}^t$.

1) DPN restoration subproblem: In this subproblem, the coupled variables $\Psi_{i,p}^t$ denote the nodal injected power $P_{i_c,G}^t$ with fast charging station (FCS) i_c, and the evacuation capacity $N_{i_b}^t$ provided for the bridging route ib. The variable $\widetilde{\Psi_{i,b}^t}$denotes the interactive information received from the EB company.

$$\begin{aligned}\min\sum_t\Delta T\Bigg[&\sum_{i\in\mathbf{V_P}/\mathbf{V_P^{couple}}}\varpi_1^{i,t}\Delta P_{i,L}^t+\sum_{i\in\mathbf{V_P^{couple}}}\varpi_2^{i,t}\Delta P_{i,L}^t\\ &+\sum_{\forall i}\lambda_i^t\left(\Psi_{i,p}^t-\widetilde{\Psi_{i,b}^t}\right)+\frac{\rho_i}{2}\left\|\Psi_{i,p}^t-\widetilde{\Psi_{i,b}^t}\right\|_2^2\Bigg]\end{aligned} \tag{84}$$

$$
\begin{aligned}
&subject\ to\\
&\begin{cases}
\mathbf{I}(\mathbf{b}_{\mathrm{p}},\mathbf{c}_{\mathrm{p}},\mathbf{\Psi}_{\mathrm{p}})\le 0,\mathbf{E}(\mathbf{b}_{\mathrm{p}},\mathbf{c}_{\mathrm{p}},\mathbf{\Psi}_{\mathrm{p}})=0\\
\mathbf{b}_{\mathrm{p}}\in\{0,1\},\mathbf{c}_{\mathrm{p}}\in[\mathbf{c}_{\min},\mathbf{c}_{\max}],\Psi_{i,p}^{t}=\{P_{i_c,G}^{t},N_{i_b}^{t}\}\\
P_{i_c,G}^{t}\in\left[\overline{P_{i_c,G}^{t}},\underline{P_{i_c,G}^{t}}\right],N_{i_b}^{t}\in\left[0,D_{i_b}^{t}\right]
\end{cases}
\end{aligned}
\tag{85}
$$

2) EBSP subproblem: In this subproblem, the coupled variables $\Psi_{i,b}^{t}$ represent the aggregated injected discharging power $p_{i_c}^{t}$ of EB fleets at the FCS ic, and the aggregated evacuation capacity $n_{i_b}^{t}$ of EB fleets provided for the bridging route ib. The variable $\widetilde{\Psi_{i,p}^{t}}$denotes the interactive information received from the DPN company.

$$
\begin{aligned}
\min\sum_{t}\Delta T\Bigg[&\sum_{m}\left(\overline{soc_m}-soc_m^{t}\right)\\
&+\sum_{i}\left(\lambda_i^{t}\left(\widetilde{\Psi_{i,p}^{t}}-\Psi_{i,b}^{t}\right)+\frac{\rho_i}{2}\left\|\widetilde{\Psi_{i,p}^{t}}-\Psi_{i,b}^{t}\right\|_2^2\right)\Bigg]
\end{aligned}
\tag{86}
$$

$$
\begin{aligned}
&subject\ to\\
&\begin{cases}
\mathbf{I}(\mathbf{b}_{\mathrm{b}},\mathbf{c}_{\mathrm{b}},\mathbf{\Psi}_{\mathrm{b}})\le 0,\mathbf{E}(\mathbf{b}_{\mathrm{b}},\mathbf{c}_{\mathrm{b}},\mathbf{\Psi}_{\mathrm{b}})=0\\
\mathbf{b}_{\mathrm{b}}\in\{0,1\},\mathbf{c}_{\mathrm{b}}\in[\mathbf{c}_{\min},\mathbf{c}_{\max}],\Psi_{i,b}^{t}=\{p_{i_c}^{t},n_{i_b}^{t}\}\\
p_{i_c}^{t}=\sum_{m\in\mathbf{B}}\left(p_{mt}^{i_c,\mathrm{dch}}-p_{mt}^{i_c,\mathrm{ch}}\right)\\
n_{i_b}^{t}\le C_m\cdot\sum_{m\in\mathbf{B}}\left(\alpha_m^{i_b}+\alpha_m^{i_b}\right)
\end{cases}
\end{aligned}
\tag{87}
$$

B. Distributed Algorithm

Due to the constraints of integer variables, the original MILP model is nonconvex and discontinuous, posing challenge to the convergence of the distributed algorithm. To address this, we devise an Iterative Alternating Optimization (IAO) with a nested Alternating Direction Method of Multipliers (ADMM). The flowchart of the algorithm is shown in Fig.9 and the theoretical analysis of this type of algorithm can be found in [35]-[37]. The key idea is to optimize the problem over repair crew and EB schedule variables, and DPN switching states (integer variables), and other DPN operating variables, while keeping the discharging and charging power of EB, and evacuation capacity for bridging routes (coupled variables) fixed. The problem is then optimized over coupled variables with the integer variables fixed, and this process is repeated iteratively. The solution procedures for IAO (algorithm 1) and ADMM (algorithm 2) are detailed as follows.

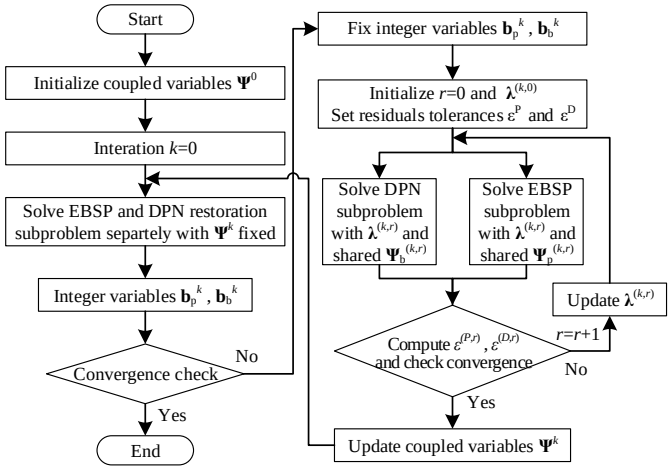

Fig. 9. Flowchart of the proposed IAO algorithm

Algorithm 1 Iterative alternating optimization (IAO)

1) Initialize. Convert the integrated MILP model (82)-(83) into a linear program (LP) by relaxing integer variables to continuous variables. Apply ADMM (algorithm 2) to achieve the decentralized solving of two subproblems. This provides the initial values of coupled variables $\mathbf{\Psi^0}$ for the DPN and EB company, where $\mathbf{\Psi}_{\mathrm{p}}^{0}$=$\mathbf{\Psi}_{\mathrm{b}}^{0}$. Set iteration $k=0$.

2) Solve Ψ-fixed subproblems. Solve the DPN restoration subproblem (84)-(85) with $\mathbf{\Psi}_{\mathrm{b}}^{k}$ fixed to $\widetilde{\mathbf{\Psi}}_{\mathrm{b}}^{k}$, and solve the EBSP subproblem (86)-(87) with $\mathbf{\Psi}_{\mathrm{p}}^{k}$ fixed to $\widetilde{\mathbf{\Psi}}_{\mathrm{p}}^{k}$, obtaining the integer variables $\mathbf{b}_{\mathrm{p}}^{k}$ and $\mathbf{b}_{\mathrm{b}}^{k}$, as well as other decision variables.

3) Check convergence. If $k>0$ and the integer variables do not change between two adjacent iterations, i.e, $\mathbf{b}_{\mathrm{p}}^{k}=\mathbf{b}_{\mathrm{p}}^{k-1}$ and $\mathbf{b}_{\mathrm{b}}^{k}=\mathbf{b}_{\mathrm{b}}^{k-1}$, the iteration terminates and outputs the solution $\left\{\mathbf{b}_{\mathrm{p}}^{k},\mathbf{b}_{\mathrm{b}}^{k},\mathbf{c}_{\mathrm{p}}^{k},\mathbf{c}_{\mathrm{b}}^{k},\mathbf{\Psi}_{\mathrm{p}}^{k},\mathbf{\Psi}_{\mathrm{b}}^{k}\right\}$. Otherwise, go to step 4).

4) Solve integer-fixed subproblems by ADMM. With integer variables $\mathbf{b}_{\mathrm{p}}^{k}$ and $\mathbf{b}_{\mathrm{b}}^{k}$ fixed, the original integrated MILP is equivalent to an LP. This allows the DPN restoration subproblem and EBSP subproblem to be solved in a fully distributed manner by the iterative ADMM (algorithm 2) with finite convergence, obtaining the values of coupled variables $\mathbf{\Psi}^{k}$. Set iteration $k=k+1$ and go to step 2).

Algorithm 2 ADMM for fully decentralized operation

1) Initialize. Set iteration $r=0$ and initialize lagrangian multipliers $\lambda^{(k,0)}$ and shared information $\mathbf{\Psi}^{(k,0)}$ for the two subproblems. Set the maximum number of iterations $R>0$, and the ADMM residuals tolerances $\varepsilon^{\mathrm{P}}>0$ and $\varepsilon^{\mathrm{D}}>0$.

2) Information exchange. The DPN company sends $\widetilde{\mathbf{\Psi}}_{\mathrm{p}}^{(k,r)}$ to the EB company. In return, the EB company sends $\widetilde{\mathbf{\Psi}}_{\mathrm{b}}^{(k,r)}$ to the DPN company.

3) Subproblems computations. Solve the DPN restoration subproblem (84)-(85) and EBSP subproblem (86)-(87) with $\lambda^{(k,r)}$ and the shared information of coupled variables, respectively, obtaining $\mathbf{\Psi}^{(k,r)}$.

4) Convergence check. Compute the primal and dual residues: $\varepsilon^{(P,r)}=\left\|\mathbf{\Psi}_{\mathrm{p}}^{(k,r)}-\mathbf{\Psi}_{\mathrm{b}}^{(k,r)}\right\|_2^2$, $\varepsilon^{(D,r+1)}=\left\|\mathbf{\Psi}_{\mathrm{b}}^{(k,r)}-\mathbf{\Psi}_{\mathrm{b}}^{(k,r-1)}\right\|_2^2$. If $\varepsilon^{(P,r)}\le\varepsilon^{\mathrm{P}}$ and $\varepsilon^{(D,r)}\le\varepsilon^{\mathrm{D}}$ or $r>R$, algorithm terminates and output the optimal solution of $\mathbf{\Psi}^{(k,r)}$.

5) Lagrangian multipliers updating. $\lambda^{(k,r)}=\lambda^{(k,r-1)}+\rho\left(\mathbf{\Psi}_{\mathrm{p}}^{(k,r)}-\mathbf{\Psi}_{\mathrm{p}}^{(k,r)}\right)$. Set $r=r+1$ and go to step 2).

VII. Case Studies

This work employs the Matlab-based Gurobi 11.0 on a personal workstation with a sixteen-core i9-11900H CPU, an RTX 3080 GPU, and 64GB of RAM. The simulation case includes an IEEE 33-node system (Case I) and an IEEE 123-node system (Case II), and the computational performance is analyzed.

A. Case I: IEEE 33-Node System

1) Network Setting and Initialization: The topology and parameter setting of RTN refer to Ref [38], and those of MN are set based on complementary relationships. A modified IEEE 33-node system is adopted to simulate the operation of DPN. The detailed parameters setting for RTN and MN are listed in Appendix Table I-IV [40]. The traffic flow distribution of RTN and MN are initialized through solving TAP [30] using fmincon in MATLAB-R2023a which are shown in Appendix

Fig.1 [40]. The parameters of DPN are listed in Appendix Table V-VII and those of EB are shown in Appendix Table VIII [40], where N_B is composed of fifty-fifty basis by $\mathbf{B_s}$ and $\mathbf{B_w}$. The topological diagrams of MN, RTN, TPN and DPN are presented in Fig.10. The power supply from DPN to TPN and that from TPN to MN are shown in Table I and Table II, respectively. The capacities and geographic locations of FCSs are listed in Appendix Table IX [40]. The depot of spared EBs and RCs is located in B1.

2) Extreme Scenario: In the extreme scenario, the initial failed power lines are P2-P8, P0-P1, P6-P7, P24-P25 and P31-P5 due to deliberate attack, and their locations and repair time are listed in Appendix Table X [40] with a time step ΔT=15min. The initial nodal loads after load shedding are shown in Appendix Table XI [40]. The load loss of nodes P7, P8, P14, P15, P17 and P26 result in the outage of TPN nodes T4, T2, T5, T3 and T7. According to the functional interdependence between TPN and MN, the metro segments M3-M7, M2-M4 and M4-M8 fail, interrupting the routes M2-M4, M2-M8, and M3-M7.

The load of the failed MN routes $r \in \mathbf{R_m^{out,t}}$ would be redistributed to bridging routes $\mathbf{R_b^{r,t}}$ and inner-layer transfer routes $\mathbf{R_m^{r,t}}$. The assigned load and duration time of each route are shown in TABLE III. The duration time of each original routes is presented in Appendix Table XII [40].

TABLE I
COUPLINGS OF MN EDGES AND TPN NODES

MN Edge	TPN Nodes	MN Edge	TPN Nodes
M1-M3	(T1,T3)	M5-M6	(T5,T6)
M2-M4	(T2,T4)	M5-M9	(T5,T9)
M1-M5	(T1,T5)	M6-M10	(T6,T10)
M2-M6	(T2,T6)	M7-M9	(T7,T9)
M3-M7	(T3,T7)	M8-M10	(T8,T10)
M4-M8	(T4,T8)	M5-M6	(T5,T6)

TABLE II
COUPLINGS OF TPN NODES AND DPN NODES

TPN Node	DPN Node	TPN Node	DPN Node
T1	P10	T6	P3
T2	P8	T7	P17
T3	P15	T8	P26
T4	P7	T9	P20
T5	P14	T10	P23

TABLE III
LOAD TRANSFER OF FAILED PATHS IN CASE I

$\mathbf{R_m^{out,t}}$	$\mathbf{R_b^{r,t}}$&$\mathbf{R_m^{r,t}}$	P_k	D_k	$time_k$
M2-M4	B2-B6	0.8808	20.2584	$2\Delta T$
	B2-B5-B6	0.1192	2.7416	$2\Delta T$
M2-M8	B2-B6-B12	0.468	10.7631	$4\Delta T$
	B2-B5-B6-B12	0.1376	3.1653	$4\Delta T$
	B2-B5-B8-B11-B12	0.0796	1.8308	$6\Delta T$
	M2-M6-M10-M8	0.3148	7.2408	$2\Delta T$
M3-M7	B3-B9	1	23.07	$2\Delta T$

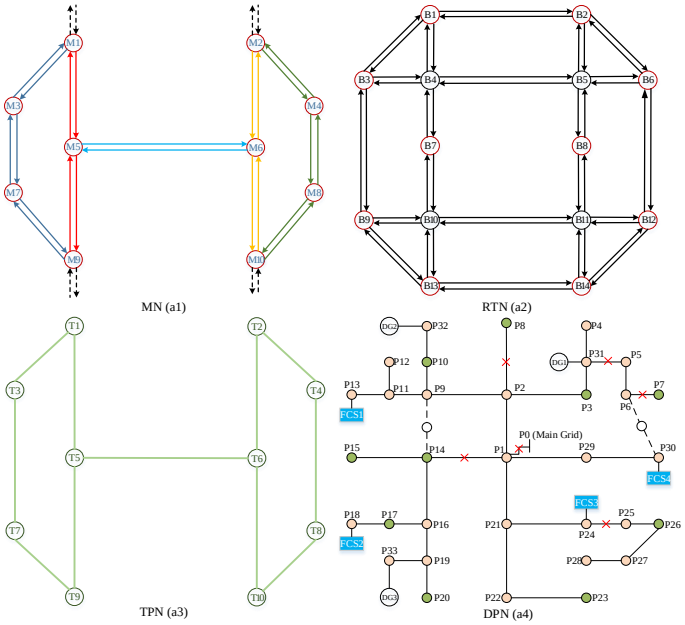

Fig. 10. The diagram of metro network (a1), road traffic network (a2), traction power network (a3) and distribution power network (a4)

3) Time cost and amount of load loss:

- Scenario 1: DPN restoration with EBs considering coupled MN demand.
- Scenario 2: DPN restoration with EBs ignoring coupled MN demand.
- Scenario 3: DPN restoration without EBs.

The DPN restoration process of above three scenarios are shown in Fig.11. Compared to scenario 3, the curtailed load recovers more quickly in scenarios 1 and 2, leading to reduced time cost of lost load through collaboration with EBs. In scenario 2, without the evacuation demand of affected MN routes, load restoration is much faster during $(4^{th}-18^{th})\Delta T$, with 0.0873MW of load restored earlier than in scenario 1 by $t = 18\Delta T$. However, in scenario 1, where the effect of unsatisfied MN traffic demand is taken into account, EBs are dispatched for bridging routes in the beginning of restoration. Furthermore, driven by the exponential growth of the time cost over time, the coupled power load is prioritized for reenergizing to recover suspended MN intervals. Their recovery sequences in scenarios 1 and 2 are listed in Table IV. Following the operational recovery of MN intervals M2-M4 and M4-M8 at $t = 7\Delta T$, the time cost increases more slowly and reaches its peak value when interval M3-M7 recovers at $t = 11\Delta T$. This peak value decreases from \$464000 in scenario 2 to \$224654 in scenario 1, underscoring the importance of prioritizing the restoration of power supply to failed MN routes.

4) Synergistic dispatch of RC and EBs: The dispatch schedule for RC and EBs is shown in TABLE V and Fig.12, respectively. According to the interdependence, the disrupted MN sections M2-M4 and M4-M8 can be supplied by T4 after the recovery of P7, making RC reach failed line P6-P7 firstly at $t = 1\Delta T$ and complete the repair at $t = 6\Delta T$. After that, 20 EBs are assigned to discharge at FCS4 to supply power to P7. Before $t = 6\Delta T$, 5 and 10 EBs are assigned to bridging routes

TABLE IV
RECOVERY SEQUENCES OF SUSPENDED MN SECTIONS IN CASE I

Considering the unsatisfied MN traffic demand			
MN sections	M2-M4	M4-M8	M3-M7
Recovery time	$t = 7\Delta T$	$t = 7\Delta T$	$t = 11\Delta T$
Without considering the unsatisfied MN traffic demand			
MN sections	M2-M4	M4-M8	M3-M7
Recovery time	$t = 13\Delta T$	t= $13\Delta T$	$t = 5\Delta T$

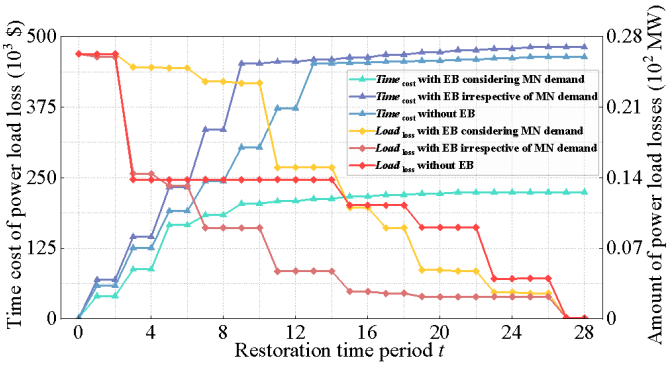

Fig. 11. Time cost and amount of load loss during restoration in Case I

i_{b4} and i_{b3} respectively during $t = 1\Delta T - 4\Delta T$ for carrying some transferred load of route M2-M8. This is because when finishing bridging services, it just takes a EB $2\Delta T$ to transfer from terminus B12 to B8 which is the location of FCS4. At $t = 17\Delta T$, 20 EBs are assigned to discharge at FCS2 to supply power to P17. EBs assigned for service trips can be divided into two types.

- EBs assigned for bridging trips $\mathbf{T_b}$ and charge-discharge trips $\mathbf{T_c}$. In particular, EB#1-EB#15 initially implement bridging service to reduce MN load loss. As shown in Table VI, such services contribute to evacuating the failed loads of M2-M8 by performing i_{b3} and i_{b4} before the recovery of disrupted section M2-M4. Then, they participate in DPN restoration with RC.
- EBs assigned for original trips $\mathbf{T_o}$ and charge-discharge trips $\mathbf{T_c}$. EB#16-EB#30 implements the above two service trips alternately. There is at least one EB for original trip at each moment to ensure the essential original transit demand.

The SOC dynamics of EB#6, EB#24, and EB#28 are portrayed in Fig.13. Taking EB#6 as an example, it is designated to perform bridging service on route i_{b3} during $t = 1\Delta T - 4\Delta T$ and arrives at FCS4 after $2\Delta T$ transfer time

TABLE V
DISPATCH SCHEDULE OF REPAIR CREW FOR FAILED LINES IN CASE I

Time(ΔT)	1-6	7-10	11-14	15-18	19-23	24-27
Failed line	P6-P7	P0-P1	P24-P25	P1-P14	P2-P8	P31-P5

TABLE VI
THE EBS DISPATHCHED FOR BRIDGING ROUTES i_{b3} AND i_{b4} IN CASE I

$\mathbf{R_b^{r,t}}$	$t = 1\Delta T$	$t = 2\Delta T$	$t = 3\Delta T$	$t = 4\Delta T$
i_{b3}	7.1%	7.1%	7.1%	7.1%
i_{b4}	0	0	0	0

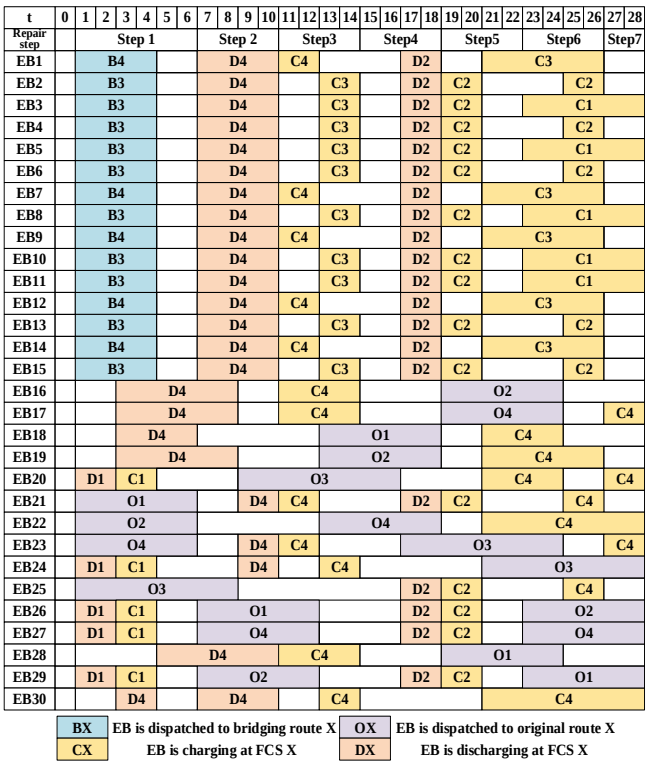

Fig. 12. Dispatch schedule of EBs for service trips in Case I

to discharge until $t = 10\Delta T$. Limited by the power supply to FCS4, EB#6 has to charge at FCS3 with a 25% SOC at $t = 13\Delta T$ and discharge at FCS2. Then, it stays at FCS2 to supplement energy until the SOC reaches 58%.

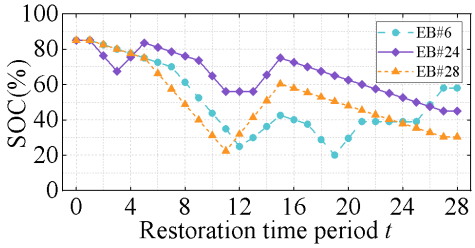

Fig. 13. SOC change of EB#6, EB#24, and EB#28 in Case I

5) Network reconfiguration: The discharging and charging behavior of EB influences its power injected or withdrawn into DPN, which further affects the network reconfiguration during restoration. The detailed restoration process is presented in Fig.14.

Initially, before the first faulted line is repaired, except for performing bridging services, 5 EBs supply power to the regular load of nodes P9-11 through FCS1. Then, four MGs are formed with the output of the other three DGs. After the recovery of P6-P7 at $t = 7\Delta T$, the tie line P6-P30 switches on, and 20 EBs flood into FCS4 to discharge, picking up the load of P7, resulting in a new MG. At $t = 11\Delta T$, the line P6-P30 that connects the main grid turns intact and the load of node P17 is restored by the power transmitted from the closed tie line P9-P14. Meanwhile, EBs start to charge at four FCSs. The charging and discharging power of FCS4 is portrayed in Fig.15. During $t = 17\Delta T - 18\Delta T$ when line P1-P14 has not been repaired, 20 EBs discharge at FCS2 to supply power to node P17 so that the load of P14 can be picked up

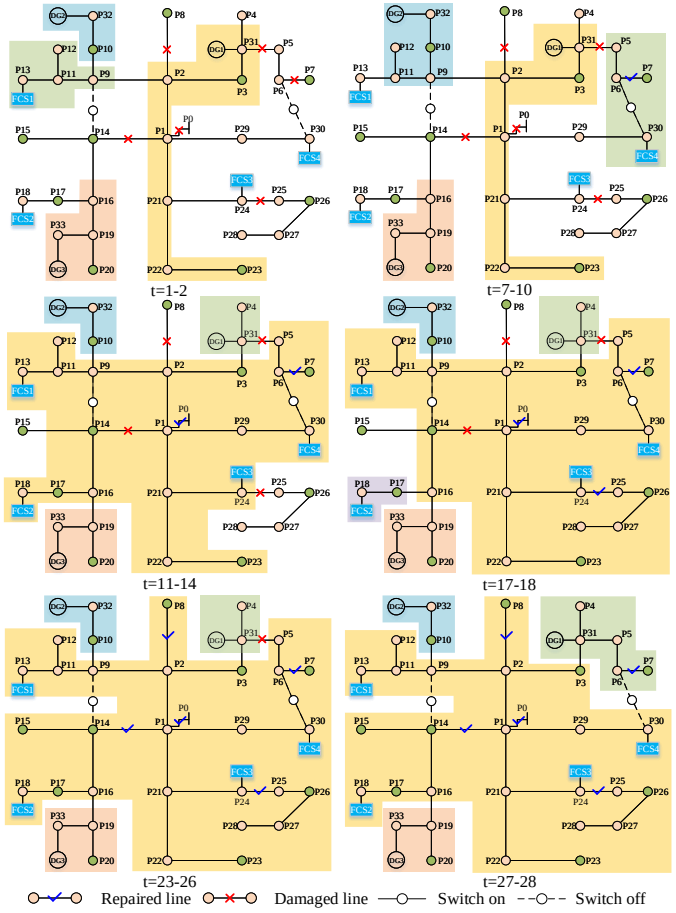

Fig. 14. DPN network reconfiguration with EBs dispatch in Case I

by the power transmitted from line P9-P14. Then, five MGs are formed. Finally, with the recovery of lines P1-P14 and P31-P5, the tie lines P6-P30 and P9-P14 are switched off.

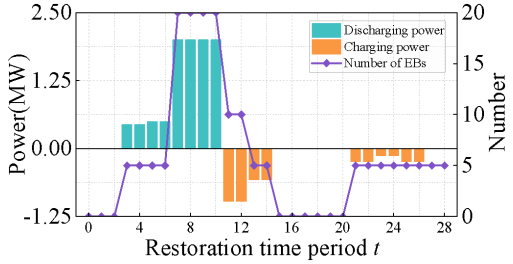

Fig. 15. Number of EBs and charge/discharge power of FCS4 in Case I

B. Case II: IEEE 123-Node System

1) Network Setting and Initialization: The topology and parameter settings of IEEE 123-node system refer to Ref [39] where the lines with zero impedance are omitted. Topologies of the MN, TPN, and RTN are detailed in the Appendix [40]. The power supply relations between MN edges and TPN nodes coincide with their numbers. For example, MN edge M1-M2 is powered by TPN nodes T1 and T2. The operating parameter and number of EB are aligned with those in the case I. The depot of spared EBs and RCs is located in B8.

2) Extreme scenario: The initial failed power lines are P0-P1, P13-P18, P13-P50, P49-P111 and P97-P101 due to deliberate attack. The load loss of nodes P4, P11, P16, P103, and P106 result in the outage of TPN nodes T4, T9, T20, T23 and T25, further disrupting the metro segments M4-M9 and M20-M25-M23. This terminates part of routes connecting Origin-Destination (OD) pairs M2-M14, M2-M19, M2-M24, M10-M23 and M15-M23. The bridging routes$\mathbf{R_b^{r,t}}$ designed for the evacuation demand of affected routes $\mathbf{R_m^{out,t}}$ are listed in TABLE VII.

TABLE VII
LOAD TRANSFER TO BRIDGING ROUTES OF FAILED PATHS IN CASE II

$\mathbf{R_m^{out,t}}$	$\mathbf{R_b^{r,t}}$	D_k	$time_k$
M20-M25-M23	B20-B25-B23	19.8005	$2\Delta T$
	B20-B18-B29-B23	2.6796	$4\Delta T$
	B20-B25-B29-B23	10.5198	$4\Delta T$
M4-M9-M14	B4-B9-B14	3.1019	$2\Delta T$
M4-M9-M14-M19	B4-B9-B14-B19	1.7942	$4\Delta T$
M4-M9-M14-M19-M24	B4-B9-B14-B19-B24	7.096	$6\Delta T$

TABLE VIII
REPAIR SEQUENCES FOR FAILED LINES IN SCENARIO 1 AND 2 IN CASE II

Time(ΔT)	1-4	5-10	11-16	17-24	25-32
Failed line	P13-P50	P49-P111	P97-P101	P13-P18	P0-P1
Time(ΔT)	1-8	9-12	13-18	19-24	25-32
Failed line	P0-P1	P13-P50	P49-P111	P97-P101	P13-P18

TABLE IX
THE EBS DISPATHCHED FOR BRIDGING ROUTES i_{b4} AND i_{b5} IN CASE II

$\mathbf{R_b^{r,t}}$	$t = 5\Delta T - 7\Delta T$	$t = 8\Delta T - 10\Delta T$
i_{b4}	EB#6-10	EB#20-24
i_{b5}	EB#1-5	EB#1-5

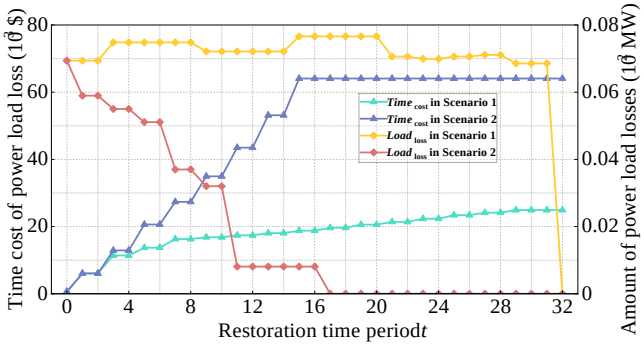

Fig. 16. Time cost and amount of load loss during restoration in Case II

3) Restoration Process:

- Scenario 1: DPN restoration with EBs considering coupled MN demand.
- Scenario 2: DPN restoration with EBs ignoring coupled MN demand.

The DPN restoration processes of these scenarios are depicted in Fig. 16, with the repair sequences of failed lines detailed in Table VIII. In scenario 1, where the effect of unsatisfied MN traffic demand is taken into account, lines P13-P50 and P49-P111 are prioritized for repair. This prioritization

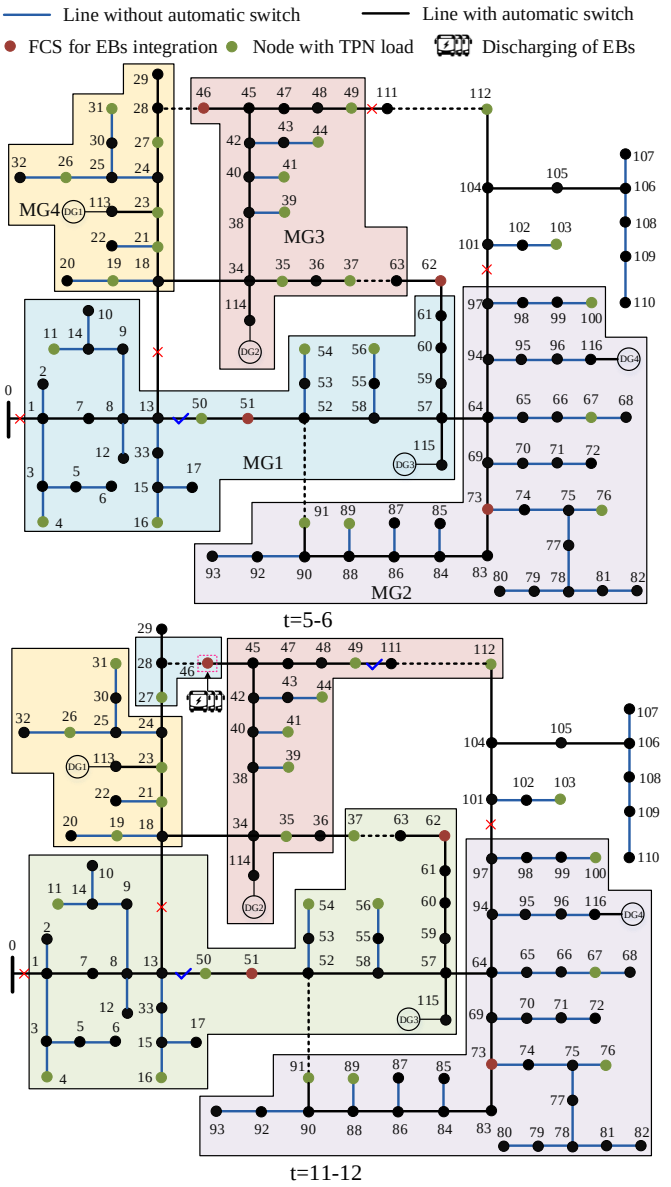

Fig. 17. IEEE 123-Node system at $t = 5\Delta T - 6\Delta T$ and $t = 11\Delta T - 12\Delta T$

restores MN links M4-M9 $t = 4\Delta T$ and M20-M25-M23 at $t = 11\Delta T$, respectively. During the period $t = 5\Delta T - 10\Delta T$, 15 EBs are dispatched to bridging routes i_{b4} and i_{b5}, fully satisfying their evacuation demands as listed in Table IX. The time cost of comprehensive load loss in scenario 1 is significantly reduced compared to that in scenario 2, decreasing from \$64062 to \$24901. However, in scenario 2, line P0-P1 is firstly recovered, contributing to quicker restorations of regular loads than that in scenario 1. This arises from the travel time required for transferring among different failed lines within a larger RTN, delaying the repair of line P0-P1 until the final moments.

The network reconfigurations at $t = 5\Delta T - 6\Delta T$ and $t = 11\Delta T - 12\Delta T$ are illustrated in Fig. 17. At $t = 5\Delta T$, the MG1 is formed upon the recovery of P13-P50. Although the output of DG3 is insufficient to jointly reenergize P4, P11 and P16, priority is given to reenergizing P4 and its coupled TPN node T25 to ensure power supply to both M20-M25 and

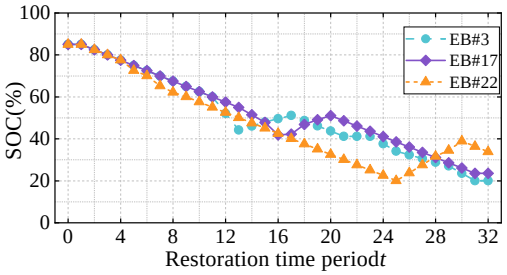

Fig. 18. SOC change of EB#3, EB#17 and EB#22 in Case II

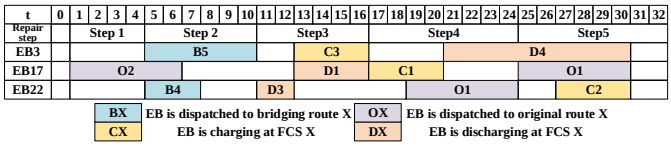

Fig. 19. Dispatch schedules of EB#3, EB#17 and EB#22 in Case II

M25-M23. Subsequently, at $t = 11\Delta T$, EBs discharge at P62 to support the load of P37 following the repair of line P49-P111, facilitating the load pickup of P112 within MG3 powered by DG2. At this point, all affected MN routes have returned to normal, allowing EBs cease bridging services and focus on load restoration. Due to the space limit, the entire DPN restoration process and the EB schedule are not elaborated upon. Dispatch plans and SOC changes of EB#3, EB#17 and EB#22 are separately presented in Fig. 19 and Fig. 18, to illustrate the transfer of EBs among their respective service trips.

C. Computational Performance Analyses of the Fast Restoration Algorithm

Computational performances comparations are conducted among the following methods: (1) the proposed original MILP (O-MILP); (2) the AIF-based MILP with two AIFs (DA-MILP) introduced in this paper; (3) the AIF-based MILP with one AIF (SA-MILP) proposed in [34]. In the AIF-based method, δ is set to 2ϕ to satisfy the condition $\delta \geq \phi$ as stipulated in [32].

The comparations results are provided in Table X, where the objective value is uniformly calculated by Eq. (26). Solving accuracy and time are significantly influenced by the gap, which controls precision in the MILP computation. However, the DA-MILP introduced in this paper can enhance the solving efficiency while guarantee the precision. In case I, the O-MILP solution reaches optimality with a 1% gap in 2679s. In contrast, both DA-MILP and SA-MILP can achieve the same optimal solution under a smaller gap of 0.1%, requiring less computation time. Testing on a larger system in case II shows that the optimal solution is reached much more quickly through DA-MILP with a 0.01% gap, which increases the computation efficiency nearly 5 times compared to O-MILP under a 0.1% gap and 4 times compared to SA-MILP under a 0.01% gap.

In practical applications, it is recommended to prioritize computational efficiency over achieving absolute solution optimality. This strategy can be realized by setting a relatively loose gap, which favoring the applicability of DA-MILP.

TABLE X
OPTIMIZATION RESULTS FOR CASE I AND CASE II

Case	Method	Gap = 1%		Gap = 0.1%		Gap = 0.01%	
		Objective Value (10^3 \$)	**Solving Time (s)**	**Objective Value** (10^3 \$)	**Solving Time (s)**	**Objective Value** (10^3 \$)	**Solving Time (s)**
I	O-MILP	224.654	2679	224.654	5896	224.654	24899
	DA-MILP	309.278	237	224.654	652	224.654	1552
	SA-MILP	271.394	489	224.654	1090	224.654	2381
II	O-MILP	26.254	3782	24.901	9852	24.901	33754
	DA-MILP	30.363	398	25.072	759	24.901	2189
	SA-MILP	28.498	631	25.165	2448	24.901	7856

TABLE XI
COMPARISON BETWEEN THE IAO SOLUTION AND THE OPTIMAL SOLUTION FOR CASE I

Time (ΔT)	**Solution of IAO**						**Optimal Solution of MILP**					
	Inject Power of FCSs (MW)				**EBs Number of ib**		**Inject Power of FCSs (MW)**				**EBs Number of ib**	
	FCS1	FCS2	FCS3	FCS4	i_{b4}	i_{b5}	FCS1	FCS2	FCS3	FCS4	i_{b3}	i_{b4}
1-2	0	0	0	0	**5**	**5**	0.5	0	0	0	**10**	**5**
3-4	0	0	0	0	**10**	**5**	-0.41	0	0	0.44	**10**	**5**
5-6	0	0	0	**0.5**	**5**	**5**	0	0	0	**0.5**	0	0
7-8	0	0	0	**0.5**	0	0	0	0	0	**2**	0	0
9-10	0	0	0	**2**	0	0	0	0	0	**2**	0	0
11-12	0	0	0	0	0	0	0	0	0	-0.97	0	0
13-14	0	0	0	0	0	0	0	0	-0.8	-0.58	0	0
15-16	0	0	0	-0.49	0	0	0	0	0	0	0	0
17-18	0	**0.2**	0	-1.01	0	0	0	**0.2**	0	0	0	0
19-20	0	0	0	0	0	0	0	-0.018	0	0	0	0
21-22	0	0	-0.42	0	0	0	0	0	-0.60	-0.24	0	0
23-24	-0.69	-0.45	-0.20	-0.50	0	0	-0.60	0	-0.03	-0.13	0	0
25-26	0	-0.26	-0.33	-0.02	0	0	-0.03	-0.60	0	-0.24	0	0
27-28	0	0	0	0	0	0	0	0	0	0	0	0
Obj	242692						224654					

D. Computational Performance and Optimality Analyses of the Distributed Method

The proposed distributed method is verified on the Case I and II. The penalty factor of the ADMM procedure ρ is set to 1. The Convergence tolerances of the primal and dual residues of the ADMM procedure are $\varepsilon^P = \varepsilon^D = 0.001$. The maximum number of iterations of ADMM is R=999.

1) Iterative Solution Process: We elaborated on the iterative solution process of IAO utilized in Case I, as illustrated in Fig. 20. In Fig. 20 (a), the max. residue denotes the largest value of primal and dual residues of all coupled variables at each ADMM iteration. It reaches the convergence tolerance in the 34th iteration when the coupled variables $\mathbf{\Psi}$ optimized by DPN company and EB company coincide. Subsequently, the loop of IAO starts, the integer variables are firstly yielded by solving $\mathbf{\Psi}$-fixed subproblems. These integer variables are then fixed, and the integer-fixed subproblems are solved with ADMM to update $\mathbf{\Psi}$, starting at the 35th iteration and converges in the 64th iteration. At this point, a new IAO round commences, and the $\mathbf{\Psi}$-fixed subproblems are solved again. Finally, the integer solutions are examined to be consistent with the previous values, allowing the IAO algorithm to terminate at the 2nd round.

In Fig. 20 (b), as one of the coupled variables of DPN restoration subproblem and EBSP subproblem, the evolution of the injected power of FCS4 at $t = 9\Delta T$ illustrates the iterative solving process of them. Initially, the DPN subproblem requires higher power injection at FCS4 to quickly restore outage loads. However, in the EBSP subproblem, EBs are reluctant to discharge at FCS4 in order to maintain their battery SOC. When the iteration terminates, the DPN company and EB company reach a consensus on the injected power of FCS4 at $t = 9\Delta T$, where both the DPN restoration and EBSP subproblems converge to 2MW.

TABLE XII
COMPUTATIONAL PERFORMANCE AND OPTIMALITY ANALYSES OF IAO

Case	Method	Objective Value (10^3\$)	Solving Time (s)
I	O-MILP	224.654	5896
	DA-MILP	224.654	652
	IAO	242.692	4483
II	O-MILP	24.901	9852
	DA-MILP	25.072	759
	IAO	26.139	8463

2) Computational Performance and Optimality Analyses: The computational time and the optimality comparisons between the IAO solution and the O-MILP optimal solution are presented in Table XII. The computational time of IAO is determined by two parts: the ADMM iterative process and the $\mathbf{\Psi}$-fixed subproblem optimization. The IAO algorithm terminates after the second round in Case I and the third round in Case II. The optimality gap primarily stems from the lack of coordination between EB scheduling and the DPN repair process. The differences between the IAO solution and the optimal

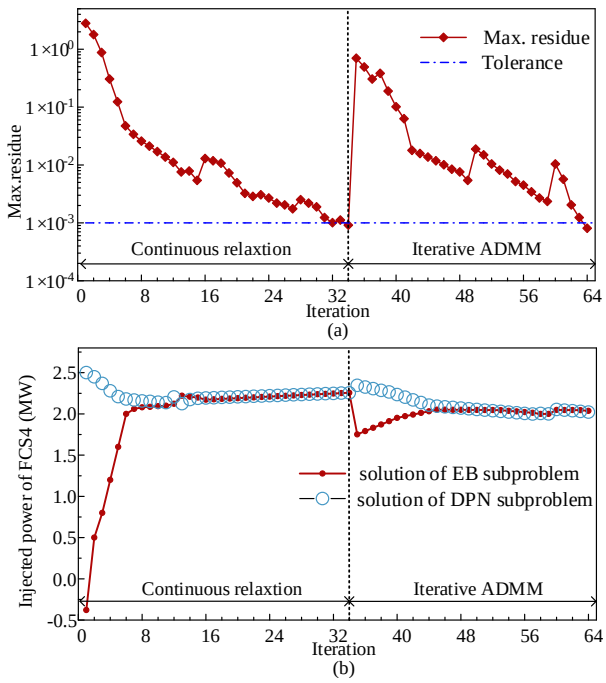

Fig. 20. Evolution of (a) the maximum residues and (b) the injected power of FCS4 at $t = 9\Delta T$ with ADMM nested in the IAO algorithm

solution in Case I are detailed in Table XI. In the IAO solutions, EBs are scheduled to perform bridging routes i_{b4} and i_{b5} during $t = 1\Delta T - 6\Delta T$, preventing 10 EBs from discharging at FCS4 to supply power to DPN node P7 at $t = 7\Delta T$ when the failed line P6-P7 is repaired. This delays the recovery of M2-M4 and M4-M8 compared to the optimal solution, which contributes to the unsatisfied evacuation demand.

The proposed distributed method can solve the original MILP, yielding a suboptimal but practically effective solution. This approach is valuable given the different authorities and interests between DPN and EB companies. However, it requires more computation time than centralized solving with the fast restoration algorithm due to the large number of iterations and the introduction of MIQP by ALD. In urban scenarios, entities are encouraged to collaborate on quick restoration with enhanced information sharing, regardless of individual interests. In practice, a centralized schedule can be implemented by the city government emergency management department.

VIII. Conclusion

This paper proposes a post-event restoration strategy for urban ETIN considering the interaction among DPN, RTN and MN through synergistically scheduling EBs and RC. Based on the dual functions of public transport and mobile power source, three post-disaster trips of EB are fully integrated in the DPN restoration model. During the multi-stage recovery of DPN, EBs are assigned to bridging services for the suspended metro intervals in the beginning. Cooperating with RC, EBs move to discharge at FCSs to supply power to the node coupled with unsatisfied MN demand on time when some critical failed lines have been repaired. Additionally, some lost regular load can be picked up by the formed microgrid based on EB discharging. With the synergistical dispatch of RC and EB, the time cost of power load loss increases much more slowly in the early stage, and its maximum value drops by more than 50 percent in both two cases. Therefore, the adverse effects of extreme events on urban ETIN are effectively addressed. Furthermore, the AIF-based fast restoration algorithm enhances the computational efficiency of the proposed model while ensuring solution optimality. The proposed distributed method solves the original MILP and yields a practically effective solution, considering individual benefits and information privacy of the DPN company and the EB company.

In the future work, the simultaneous damage to both road and DPN will be considered, and the impact of damaged roads on the travel time of EBs and RCs will be quantified to further explore their optimal schedule strategies in the post-event scenario.

References

[1] G. Liu *et al.*, "Modeling and vulnerability analysis of multi-layer urban electric-transportation interdependent networks under extreme events," *CSEE JPES.*, early access, doi: 10.17775/CSEEJPES.2022.07440.

[2] Beijing Transport Institute, "2021 Beijing Development Annual Report," Beijing Transport Institute, Beijing, CHINA, 2021.

[3] Chinese Society of Automotive Engineering, *Energy Saving and New Energy Vehicle Technologies Roadmap 2.0.* Beijing, CHINA: China Machine Press, 2021.

[4] W. Wei *et al.*, "Interdependence between transportation system and power distribution system: a comprehensive review on models and applications," *J. Mod. Pow. Sys. Clean Ener.*, vol. 7, no. 3, pp. 433-448, Apr. 2019.

[5] Y. Sheng, Q. Guo *et al.*, "A potential security threat and its solution in coupled urban power-traffic networks with high penetration of electric vehicles," *CSEE JPES.*, vol. 8, no. 4, pp. 1097-1109, Jul. 2022

[6] S. Zhang, F. Zheng *et al.*, "Thoughts on urban waterlogging control in Beijing from the rainstorm and flood of '2021.7.20' in Zhengzhou,"*China Flood & Drought Management*, vol. 31, no. 9, pp. 5-11, Sep. 2021.

[7] ANTIY Institute, CSGITSEC, "Preliminary analysis and reflections on large-scale power outage in Venezuela," *Information security and communication Privacy*, vol. 5, pp. 28-39, May. 2019.

[8] J. Jasiunas *et al.*, "Energy system resilience – A review," *Renewable and Sustainable Energy Reviews*, vol. 150, no. 111476, Oct. 2021.

[9] C. Chen, J. Wang, F. Qiu, D. Zhao, "Resilient distribution system by microgrids formation after natural disasters," *IEEE Trans. Smart Grid*, vol. 7, no. 2, pp. 958-966, Mar. 2016.

[10] M. Esteban, J. Portugal-Pereira, "Post-disaster resilience of a 100% renewable energy system in Japan," *Energy*, vol. 68, pp. 756-764, Apr. 2014.

[11] C. Gouveia, C. J. Moreira, *et al.*, "Microgrid service restoration: the role of plugged-in electric vehicles," *IEEE Industrial Electronics Magazine*, vol. 7, no. 4, pp. 26-41, Dec. 2013.

[12] Y. Xin *et al.*, "Resilience-oriented distribution system restoration considering mobile emergency resource dispatch in transportation system," *IEEE Access*, vol. 7, pp. 73899-73912, Jun. 2019.

[13] B. Taheri *et al.*, "Distribution system resilience enhancement via mobile dmergency generators," *IEEE Trans. Industrial Informatics*, vol. 17, no. 2, pp. 2308-2319, Aug. 2021.

[14] Y. Ge *et al.*, "Co-optimization approach to post-storm recovery for interdependent power and transportation systems," *J. Mod. Pow. Sys. Clean Ener.*, vol. 7, no. 4, pp. 688-695, Apr. 2019.

[15] Y. Wang, Y. Xu, *et al.*, "Dynamic load restoration considering the interdependencies between power distribution systems and urban transportation systems," *CESS JPES.*, vol. 6, no. 4, pp. 772-781, 2020.

[16] B. li *et al.*, "Resilient restoration of distribution systems in coordination with electric bus scheduling," *IEEE Trans. Smart Grid*, vol. 12, no. 4, pp. 3314-3325, Jul. 2021.

[17] B. li *et al.*, "Routing and Scheduling of Electric Buses for Resilient Restoration of Distribution System," *IEEE Trans. Transportation Electrification*, vol. 7, no. 4, pp. 2414-2428, Dec. 2021.

[18] H. Fotouhi, S. Moryadee, E. Miller-Hooks "Quantifying the resilience of an urban traffic-electric power coupled system," *Rel. Eng. Syst. Saf.*, vol. 163, no. 1, pp. 79-94, Dec. 2017.

[19] Q. Zou *et al.*, "Enhancing resilience of interdependent traffic-electric power system," *Rel. Eng. Syst. Saf.*, vol. 191, Jun. 2019.

[20] H. Wang *et al.*, "Risk assessment of an electrical power system considering the influence of traffic congestion on a hypothetical scenario of electrified transportation system in New York state," *IEEE Trans. Intelligent Transportation Systems*, vol. 22, no. 1, pp. 142-155, Jan. 2021.

[21] F. Wu, J. Yang, *et al.*, "Cascading failure in coupled networks of transportation and power grid," *Int. J. Electr. Power Energy Syst.*, vol. 140, no. 108058, Feb. 2022.

[22] H. Wang *et al.*, "Resilience-oriented optimal post-disruption reconfiguration for coupled traffic-power systems," *Rel. Eng. Syst. Saf.*, vol. 222, no. 108408, Feb. 2022.

[23] N. Goldbeck *et al.*, "Resilience assessment for interdependent urban infrastructure systems using dynamic network flow models," *Rel. Eng. Syst. Saf.y*, vol. 188, pp. 62-79, Mar. 2019.

[24] H. Liu *et al.*, "Vulnerability analysis of complementary transportation systems with applications to railway and air line systems in China," *Rel. Eng. Syst. Saf.*, vol. 142, pp. 249-257, Jan. 2015.

[25] Y. Huang *et al.*, "Coupling time-indexed and big-M formulations for real-time train scheduling during metro service disruptions," *Transp. Res. Part B: Methodological*, vol. 133, pp. 38-61, Jan. 2020.

[26] X. Wang *et al.*, "Cooperative train control during the power supply shortage in metro system: A multi-agent reinforcement learning approach," *Transp. Res. Part B*, vol. 170, pp. 244-278, Apr. 2023.

[27] W. Gu *et al.*, "Plan-based flexible bus bridging operation strategy," *Transp. Res. Part C*, vol. 91, pp. 202-229, Jun. 2018.

[28] Y. Yuan *et al.*, "Mobility-driven integration of heterogeneous urban cyber-physical systems under disruptive events," *IEEE Trans. Mobile Computing*, vol. 22, no. 2 pp. 906-922, Feb. 2023.

[29] G. Manikandan *et al.*, "Quantifying and enhancing the energy resilience of zero-emission train station systems against power outages via electrified train-building integrations," *Energy Conversion and Management: X*, vol. 22, no. 100531, Apr. 2024.

[30] W. Wei, J. Wang, "Modeling and optimization of interdependent energy," Cham, Switzerland: Springer, 2020, pp. 348-352.

[31] H. G. Yeh, D. F. Gayme *et al.*, "Adaptive VAR control for distribution circuits with photovoltaic generators," *IEEE Trans. Power System*, vol. 27, no. 3 pp. 1656-1663, Aug. 2012.

[32] Z. Yang *et al.*, "Optimal transmission switching based on auxiliary induce function," in *Proc. IEEE PES Gen. Meeting Conf. Expo.,* National Harbor, MD, USA, 2014, pp. 1–5.

[33] Y. Bai *et al.*, "Inducing-objective-function-based method for long-term SCUC with energy constraints," *Int. J. Electr. Power Energy Syst.*, vol. 63, pp. 971-978, Dec. 2014.

[34] T. Ding *et al.*, "Multiperiod distribution system restoration with routing repair crews, mobile electric vehicles, and soft-open-point networked microgrids," *IEEE Trans. Smart Grid*, vol. 11, no. 6, pp. 4795-4808, Nov. 2020.

[35] Z. G. Li *et al.*, "Decentralized multiarea robust generation unit and tie-line scheduling under wind power uncertain," *IEEE Trans. Sus. Energy*, vol. 6, no. 4, pp. 1377-1388, Oct. 2015.

[36] Y. B. He *et al.*, "Decentralized optimization of multi-area electricity-natural gas flows based on cone reformulation," *IEEE Trans. Power System*, vol. 33, no. 4, pp. 4531-4542, July 2018.

[37] Z. Chen *et al.*, "Fully distributed robust reserve scheduling for coupled transmission and distribution systems," *IEEE Trans. Power System*, vol. 36, no. 1, pp. 169-182, Jan. 2021.

[38] W. Wei *et al.*, "Optimal traffic-power flow in urban electrified transportation networks," *IEEE Trans. Smart Grid*, vol. 8, no. 1, pp. 84-95, Jan. 2017.

[39] Q. Shi *et al.*, "Preventive allocation and post-disaster cooperative dispatch of emergency mobile resources for improved distribution system resilience," *Int. J. Electr. Power Energy Syst.*, vol. 152, no. 109238, Oct. 2023.

[40] R. Cheng, "Appendix-of-Enhancing-Resilience," Accessed: Oct. 2024. [Online]. Available:https://github.com/RuiCheng94/Appendix-of-Enhancing-Resilience/issues/1.

Gengming Liu received B.S. degree in Electrical Engineering and Automation from North China Electrical Power University in 2019. He is currently working towards doctor degree in the School of Electric and Electronic Engineering, North China Electrical Power University, Beijing, China. His major interests include vulnerability analysis and resilience enhancement of interdependent electric-traffic system and cyber-physical power system security.

Rui Cheng (Member, IEEE) is currently the Assistant Professor at North China Electric Power University. He received the Ph.D. degree in electrical engineering from Iowa State University in 2023. He was the recipient of the Best Paper Award from the IEEE Power & Energy Society General Meeting, and the Research Excellence Award from Iowa State University. His research interests include optimization and machine learning in power distribution systems, and power system vulnerability and reliability.

Wenxia Liu (Member, IEEE) received B.S. degree in Radio technology from Nanjing University of Science and Technology in 1990, and obtained M.S. degree and PhD degree in Electrical Engineering and Automation from Northeast of China Electrical power University and North China Electrical Power University in 1995 and 2009, respectively. She is currently professor in the School of Electric and Electronic Engineering, North China Electrical Power University, Beijing, China. Her research interests include risk assessment in power system, cyber-physical power system security.

Qingxin Shi (Member, IEEE) received the B.S. and M.Sc. degrees from Zhejiang University, China, and University of Alberta, Canada, in 2011 and 2014, respectively. He received the Ph.D. degree in 2019 from the University of Tennessee, Knoxville, USA, where he worked as a research assistant professor until 2020. He is working as an associate professor in North China Electrical Power University, Beijing, China. His research interests include demand response and distribution system resilience.

Zhaoyu Wang (Senior Member, IEEE) received the B.S. and M.S. degrees in electrical engineering from Shanghai Jiao Tong University, and the M.S. and Ph.D. degrees in electrical and computer engineering from Georgia Institute of Technology. Since 2015, he has been assistant, associate, and full Professor at Iowa State University. His research interests include optimization and data analytics in power distribution systems and microgrids. He was the recipient of the National Science Foundation CAREER Award, the IEEE Power and Energy Society (PES) Outstanding Young Engineer Award, the Northrop Grumman Endowment, College of Engineering's Early Achievement in Research Award, and the Harpole-Pentair Young Faculty Award Endowment. He is the lead Principal Investigator for over $23M projects funded by the National Science Foundation, the Department of Energy, National Laboratories, PSERC, and Iowa Economic Development Authority. He is the Technical Committee Program Chair (TCPC) of IEEE Power System Operation, Planning and Economics (PSOPE) Committee, the Vice Chair of IEEE Distribution System Operation and Planning Subcommittee, the Secretary of IEEE Task Force on IEEE P3102 Standard for Conservation Voltage Reduction (CVR) Data Collection and Management Procedures, and the Vice Chair of IEEE Task Force on Advances in Natural Disaster Mitigation Methods. He is an Associate Editor of IEEE TRANSACTIONS ON SUSTAINABLE ENERGY, IEEE OPEN ACCESS JOURNAL OF POWER AND ENERGY, IEEE POWER ENGINEERING LETTERS, and IET Smart Grid. He was an Associate Editor of IEEE TRANSACTIONS ON POWER SYSTEMS, IEEE TRANSACTIONS ON SMART GRID, and the Chair of PSOPE Awards Subcommittee.